Assessment of Hg speciation changes in the sedimentary rock record from thermal desorption characteristics

Frieling, J.[1*], Fendley, I.M.[1,2*], Nawaz, M.A.[1] and Mather, T.A.[1]

[1] Department of Earth Sciences, University of Oxford, Oxford, OX1 3AN, UK

[2] Department of Geosciences, Pennsylvania State University, University Park, PA 16802, USA

*Corresponding authors; Joost Frieling (joost.frieling@earth.ox.ac.uk), Isabel Fendley (ifendley@psu.edu)

Key Points:

- Our ability to resolve the processes driving sedimentary Hg concentrations is affected by (changes in) Hg speciation in sedimentary rocks
- Via the use of thermal desorption characteristics, we developed a method to simultaneously obtain total Hg and Hg speciation for each sample
- Multiple phases of Hg release occur and the individual phases vary in importance between samples

Abstract

Sedimentary mercury (Hg) has become a widely used proxy for paleo-volcanic activity. However, scavenging and drawdown of Hg by organic-matter (OM) and sulfides are important non-volcanic factors determining variability in such records. Most studies, therefore, normalize total Hg (Hg_T) to a Hg "host-phase" proxy (e.g., Hg_T/TOC for OM, Hg_T/TS for sulfides), with the dominant host-phase determined based on the strongest observed (linear) correlations. This approach suffers from various non-linearities in Hg-host-phase behavior and does not account for succession-level, let alone sample-level, Hg speciation changes. Thermal desorption characteristics or 'profiles' (TDPs) for many Hg species during pyrolysis analysis are well-established with applications including distinguishing between OM-bound Hg and different Hg sulfides and oxides in (sub-)recent sediments. We explore the use of TDPs for geological sediment (rock) samples and illustrate the presence of multiple release phases (Hg species) – correlated to

geochemical host-phase – in (almost) all the 65 analyzed Tithonian (146 – 145 Ma) silt and mudrock samples. By quantifying the Hg in each release phase for every sample, we find TOC concentration may determine ~60% of the variability in the first (lower temperature) Hg TDP release phase: a stark difference with the total Hg released from these samples, where ~20% of variation is explained by TOC variability. TDPs provide insight on sample-level Hg speciation and demonstrate that, while the common assumption of single-phase Hg speciation in sedimentary rocks is problematic, differences in Hg speciation can be detected, quantified, and accounted for using commonly applied techniques - opening potential for routine implementation.

Plain Language Summary

Sedimentary mercury (Hg) has become a widely used proxy for paleo-volcanic activity. The concentration of Hg in sediments is however also impacted by a combination of non-volcanic processes and most notably the abundance of Hg-scavenging phases such as organic-matter or sulfides. The Hg host phase, closely linked to Hg speciation, has been almost exclusively defined based on the strongest linear correlations, without independent control or validation of the key assumptions that Hg is hosted in a single phase (i.e., is present in a single chemical species) and or that this can be determined via correlation. We here test whether ramping desorption temperatures of sedimentary Hg species can provide a feasible path to Hg speciation constraints for each individual sediment rock sample. With limited additional effort, we obtained these thermal desorption data simultaneously with total Hg concentration values. Virtually all upper Jurassic sediment samples in our test set show the presence of multiple Hg phases, in conflict with the common assumption of single-phase Hg speciation. The thermal desorption approach presented here provides a simple independent method to gain a new perspective on some of the key assumptions that underlie the use of Hg as a proxy for paleo-volcanic activity.

1 Introduction

Mercury is released into and cycled through the atmosphere-ocean system by various geological, geogenic, anthropogenic and biological processes (Lyman et al., 2020). Geological release processes include natural heating of sedimentary rocks (coal/other hydrocarbon combustion), erosion of Hg-bearing rocks, and notably via volcanic and hydrothermal activity (Selin, 2009). Among these naturally occurring processes, volcanic Hg emissions are a major component with an estimated flux of 76 – 700 metric tons yr^{-1} (Bagnato et al., 2015; Geyman et al., 2023; Pyle & Mather, 2003). Most volcanic mercury emissions are in the form of gaseous elemental mercury, which has an atmospheric residence time of up to 2 years (Lyman et al., 2020), enabling hemispheric or even global distribution (Selin, 2009). Following deposition from the atmosphere (e.g., Jiskra et al., 2021), Hg is assumed to be scavenged and sequestered into sediments and held in absorbed or chemically bound form by a host-phase. Together with the host-phase, typically assumed to be organic-matter (OM), sulfur groups within OM (thiols) or sulfides, Hg is ultimately stored in the geological record (e.g., Ravichandran, 2004; Fitzgerald et al., 2007; Amos et al., 2014). Mercury is generally assumed to be primarily hosted by OM upon deposition in aquatic sediments (Wallace, 1982), and this is widely supported by Hg data from soft sediments. However, it is also well-established that, even when OM-associated, Hg can be hosted by other (OM-associated) phases (Pham et al., 2014) and that OM may not always be the dominant host in all environments. Furthermore, the association with diagenetic pyrites shows that Hg speciation can change after deposition and (burial) diagenesis (Shen et al., 2019; Zhao et al., 2022).

Mercury speciation determines how (im)mobile Hg might be during erosion (Manceau et al., 2018) or upon heating, such as during hydrocarbon formation, production and burning (Yudovich & Ketris, 2005), but also soils subjected to intense forest fires (Biswas et al., 2007), and sediments near intrusive and eruptive volcanic activity (Chen et al., 2022; Liu et al., 2022; Svensen et al., 2023; Zaputlyaeva et al., 2020). It is difficult to gauge the importance of geological Hg fluxes from any of these potential sources without knowledge of Hg speciation in (sedimentary) rocks.

1.1 Sedimentary Hg host-phases and use of Hg as a paleo-volcanic proxy

In addition to environmentally relevant Hg sources, sedimentary Hg has become a widely applied proxy for large-scale paleo-volcanic activity, particularly large igneous province (LIP)

volcanism. To do so, most studies make the *a priori* assumption that, through time, variations in sedimentary Hg concentration are primarily controlled by the abundance of a Hg host-phase. The abundance of these host-phases is typically estimated from parameters such as total organic carbon (TOC, a proxy for OM), total sulfur (TS, often used as a proxy for sulfides but also includes organic-S and sulfates) or aluminum concentrations (a proxy for clay abundance). The host-phases for Hg are closely linked to Hg speciation but it is important to note that Hg speciation typically refers to the chemical species of Hg (e.g., methylated Hg, HgS, HgO) and their relative importance and that, for example, a single Hg "host-phase" such as OM or pyrite can be composed of several Hg-species. In order to seek out enhanced Hg loading, almost all studies to date have 'normalized' total Hg (Hg_T) to a geochemical parameter that serves as a proxy for a particular host-phase. Identifying the host-phase has largely relied on linear correlation for multi-million-year successions and across severe environmental perturbations by assuming the strongest correlation with another analyzed parameter (usually TOC or TS) reflects the dominant host-phase for all analyzed samples (e.g., Percival et al., 2015; Grasby et al., 2019; Zhao et al., 2022).

There is theoretical and empirical support for this approach. The abundance of particulate and dissolved OM is an important factor in controlling the Hg levels in seawater (Wallace, 1982) and during sequestration in sediments (Fitzgerald et al., 2007; Gehrke et al., 2009; Outridge et al., 2007). This relationship is due to the very high affinity of Hg^{2+} for OM and organic sulfur functional groups (thiols) (see, e.g., review of Ravichandran, 2004), which commonly leads to strong correlations between TOC and Hg (Gehrke et al., 2009; Outridge et al., 2007). In these cases, the correlation between Hg and TOC supports OM as the host-phase of the Hg within the sediment (wherein the Hg is likely chemically bound in organic compounds and minerals). Provided redox and diagenetic conditions and the Hg and TOC flux are unchanged over the analyzed sequence (Frieling et al., 2023; Grasby et al., 2013; Shen et al., 2020), this should then lead to a stable Hg_T/TOC in soft and lithified sediments. Anomalies above a Hg_T/TOC baseline have most commonly been attributed to an increased Hg flux, the strongest of which may then be attributed to elevated volcanic activity in large igneous provinces (LIPs) (Percival et al., 2015; Sanei et al., 2012). As the use of sedimentary Hg as a proxy for (LIP) volcanism has become more prevalent, several inherent complexities that may influence Hg_T signals in the geological record have come to light. Many of these issues are centered around the Hg-host phase relationship.

Until now, studies have been mostly limited to statistical correlations to derive the (dominant) sedimentary host-phase of Hg. This is especially challenging as proposed Hg carriers (OM, sulfides, and clays) tend to be inherently coupled or co-varying in sedimentary records and at the same time are heterogeneous compounds. In reducing conditions, including anoxic and euxinic environments, Hg can be present as HgS or be hosted by sulfide minerals such as pyrite (adsorbed or as HgS) (Manceau et al., 2018; Pham et al., 2014), and for lithified samples, elemental mapping yielded evidence of pyrite-hosted Hg (Shen et al., 2020; Z. Wang et al., 2020). Lastly, in settings where other scavenging ligands are rare or difficult to analyze, other sediment constituents such as iron-oxides and clay fractions have been proposed to serve as Hg hosts (e.g., Percival et al., 2018).

Whilst normalizing to the best-correlating host-phase proxy parameter (TOC, TS, Al) is currently common practice, there are important shortcomings and challenges with this approach that affect the interpretation of the geological Hg_T record. First, even a perfect linear correlation does not always signal that Hg loading was driven by host-phase abundance. Variable mixing of low-Hg_T, low-TOC and high-Hg_T, high-TOC phases would also impose such a correlation. End-member mixing effects could be imposed by, for example, carbonate or siliciclastic fractions and impact the geological record (Fendley et al., in press; Frieling et al., 2024). Second, the host-phase relation can be complicated by variable fluxes in Hg or TOC, S or clay, which could induce a system change from receptor (Hg burial limited by the availability of the scavenging/host-phase) to flux limitation (Hg burial limited by the availability of Hg) (e.g., Fendley et al., in press; Frieling et al., 2023; Machado et al., 2016; Schuster et al., 2018). Such systematic changes can result in non-linearity of the Hg-host relation. Non-linearity typically expresses as strongly inflated Hg-host phase normalized values when host-phase abundance is low and suppressed normalized Hg when host-phases are abundantly present (Fendley et al., in press; Frieling et al., 2023; Schuster et al., 2018).

In light of these complexities, perhaps the most problematic and fundamental assumption is that Hg is typically assumed to be bound within a single dominant host-phase throughout a succession and that this phase can be identified via (linear) correlation. As (sub-)recent sediments often show strong spatial and temporal heterogeneity in Hg speciation (e.g., Chakraborty et al., 2014; Gamboa Ruiz and Tomiyasu, 2015; Lim et al., 2020; Wilman et al., 2023) it is likely that the same applies to the geological record and that the importance of various Hg species and hence

host-phases (subtly) changes through the analyzed successions. The likelihood of changing speciation increases when the analyzed sequences span substantial environmental perturbations that are often accompanied by broad biogeochemical and lithological changes, which is inherent to the vast majority of the records to which Hg_T is applied as a paleo-volcanic proxy (e.g., Grasby et al., 2019). Single-variable normalization aids in removing part of the host-phase driven variability, but it inevitably also introduces false variability in other sections or for single samples. An extreme example of this would be Hg focusing in diagenetic pyrite beds (Gong et al., 2017; Shen et al., 2019). In this case, if one assumed that Hg was hosted by a single dominant (non-pyrite) phase throughout a succession and remained unaware of the focusing effect, then the natural conclusion would be that environmental Hg loading was variable (Gong et al., 2017). In another scenario, the dominant host-phase may switch from OM to pyrite between samples in a binary fashion within a section. If normalized exclusively to either host Hg levels might look as if they varied but in fact the conclusion that no change in environmental Hg loading occurred could be equally valid (Shen et al., 2019).

While linear single-variable host-phase normalizations for entire successions may be crude, they have provided insight into the most severe Hg cycle changes in deep time (Jones et al., 2019; Percival et al., 2017; Sanei et al., 2012). The complexities and pitfalls that surround host-phase identification based on correlation alone are however obvious and require close attention to increase our skill in identifying and quantifying more subtle changes in past Hg cycling. We therefore seek to expand knowledge on the Hg_T host-phase relation by applying methodology that is less dependent on succession-level characteristics and correlations with other data, in an attempt to avoid some of the confounding factors that hamper proper Hg-host phase determination. Specifically, we aim to test whether constraints on Hg speciation can help inform whether host-phase correlations and normalizations are justified.

1.2 Hg speciation techniques

Existing techniques to directly determine Hg speciation can be broadly divided into categories that center on chemical (sequential) extraction, mineral identification, element mapping and thermal desorption. Sequential extraction techniques have been developed using solubilizing of Hg from Hg-binding phases (Gleyzes et al., 2002; Issaro et al., 2009). The main strength of sequential extraction is that it can distinguish between many Hg species. However, the analyses

are generally time-consuming, and can suffer from variable recovery due to volatility of Hg and solubility characteristics of some phases (Bloom et al., 2003; Issaro et al., 2009; Kim et al., 2003).

Studies have applied synchrotron or other mineral-identification techniques of Hg rock samples, but these approaches are best suited to material with >ppm-level Hg concentrations, typically encountered in ore minerals and very rare in sedimentary rocks (Kim et al., 2003). Energy dispersive spectroscopy (EDS) element mapping can be sensitive enough to detect concentrated Hg in samples with sub-ppm total Hg concentrations. Mapping is a powerful tool that may identify which (mineral) phases concentrate elements, and this has established, for example, that, besides typical Hg ores, (diagenetic) pyrite in sediments may hold significant amounts of Hg (e.g., Shen et al., 2019; Y. Wang et al., 2023; Z. Wang et al., 2020). Translating the Hg from two-dimensional element mapping to relative proportions of Hg hosted by specific phases for an entire sample, however, remains a challenge. In addition, this approach is time-consuming, such that realistically it cannot be applied to the sometimes >100s of samples that are often analyzed for a single study.

To expand to the sample volume often required to make inferences of geological Hg cycling, a more promising category for rapid Hg speciation of rock samples is the use of thermal properties of Hg species to disentangle Hg speciation (e.g., Bombach et al., 1994). Many dedicated Hg analyzers are based on pyrolysis-based methods, whereby the sample material is rapidly heated to a temperature where most naturally occurring Hg species are desorbed (>700 ºC). The Hg is quantified through atomic absorption spectroscopy, with or without an intermediate step where Hg is amalgamated onto gold (gold trapping) (e.g., Enrico et al., 2020). Over the past decades, several studies have established and utilized thermal desorption profiles (TDPs) of Hg species, including, for example, elemental Hg, OM-bound Hg, HgS ((meta-)cinnabar), HgO (montroydite), $HgSO_4$ and HgSe (tiemannite) to determine their abundance in natural and polluted sediment samples (e.g., Bombach et al., 1994; Biester and Scholz, 1997; Rumayor et al., 2013; Rumayor et al., 2015; Saniewska and Bełdowska, 2017; Bełdowska et al., 2018; Petranich et al., 2022, Table 1). With a focus on environmental Hg and the adverse ecological effects of certain Hg species, these studies have generally applied step-wise or gradual, shallow, temperature ramps to monitor the release of Hg species with increasing temperature. A relatively shallow temperature ramp is potentially beneficial as it may limit concurrent Hg release from multiple species (Bełdowska et al., 2018; Reis et al., 2015). Although less precise in determining the exact Hg species compared to sequential extraction or element mapping, due to overlapping desorption temperatures of

compounds, thermal desorption has proven potential to reliably detect and resolve changes in relative abundances of most common naturally occurring Hg species (Biester & Nehrke, 1997). Crucially, this technique requires limited or no (chemical) pre-treatment, analysis time is typically ~minutes per sample and the method is broadly and directly applicable as the majority of Hg data for geological proxy work are generated using pyrolysis-based methods.

1.3 Study aims & approach

It is evident that information on Hg speciation is required on a sample level to test whether and to what extent the assumptions on host-phase behavior and host-phase normalization that form the basis of Hg as a proxy for paleo-volcanic activity are justified. We emphasize that it is our intention to develop a method to assess fundamental aspects of the Hg data that should be followed by – but not replace – further rigorous statistical testing for potentially anomalous Hg concentration values, appropriate host-phase normalized values and Hg mass accumulation rates to infer enhanced paleo-volcanic activity.

To this end, we test whether the detailed knowledge of the thermal behavior of Hg species can be widely employed to provide insight into Hg speciation in individual geological samples. First, we determine whether Hg thermal desorption from lithified sediment samples varies systematically, and how these variations might manifest. Subsequently, we examine whether the thermal desorption during total Hg measurement via the rapid pyrolysis-based methods that are commonly used to determine Hg_T in geological samples (< 3 minutes per sample), rather than the much longer (>>10 minute) temperature ramps or thermo-scanning common in environmental sciences (e.g. Saniewska & Bełdowska, 2017), can be used as a screening tool or even a basic quantitative estimate of Hg speciation in geological samples. Establishing such a method could provide a feasible way to monitor Hg speciation (changes) for each analyzed sample with limited additional effort, at the same time as Hg_T is obtained.

For the purpose of testing and establishing such a method and in order to understand the background variability before applying it to more complex time spans, we selected a set of sedimentary rock samples that are thought not to be associated with any known LIP activity. Thus, we analyzed multiple aliquots of three different standard materials to assess reproducibility, and a set of sedimentary rock samples from the Tithonian Kimmeridge Clay Formation (KCF) (Late Jurassic, *ca.* 146 – 145 Ma). Astronomically-paced environmental changes drive the main

lithological variability in this sedimentary succession from the Swanworth Quarry borehole, UK (Huang et al., 2010; Weedon et al., 1999) and no large-scale volcanic events (e.g., Ernst et al., 2021) or local activity that may have resulted in variable environmental Hg loading is known for this period.

2 Materials and Methods

2.1 Materials

The natural geological samples analyzed for this study were obtained from a cored borehole at Swanworth Quarry (SQ-1) (50.604 ºN, -2.044 ºE). The SQ-1 bore hole, together with a second bore hole at the same location and one at Metherhills (50.613 ºN, -2.123 ºE), represents a near-complete record of the Kimmeridge Clay Formation (KCF) (Morgans-Bell et al., 2001) (Fig.1). Deposited in the Wessex Basin (present-day United Kingdom) during the Upper Jurassic Kimmeridgian and Tithonian stages (*ca.* 153 – 145 Ma), it was inferred from various sediment proxy data (pyrite framboids, uranium enrichment and biomarkers signaling the presence of photosynthesizing green sulfur bacteria) that intervals of the KCF were deposited in anoxic-euxinic bottom waters (Van Kaam-Peters et al., 1998; Raiswell et al., 2001; Tyson et al., 1979). Besides strata deposited under anoxic conditions, the formation comprises a range of lithologies including mudstones, marls, and shales with lesser amounts of limestones, siltstones and dolostones. The cyclical deposition of these facies and the environmental changes they reflect is thought to be the product of orbital forcing (Huang et al., 2010; Weedon et al., 1999). The KCF represents a range of natural conditions deposited without significant local volcanic events or LIP

emplacement, and we therefore assume changes in environmental Hg loading and speciation are the result of non-volcanic processes.

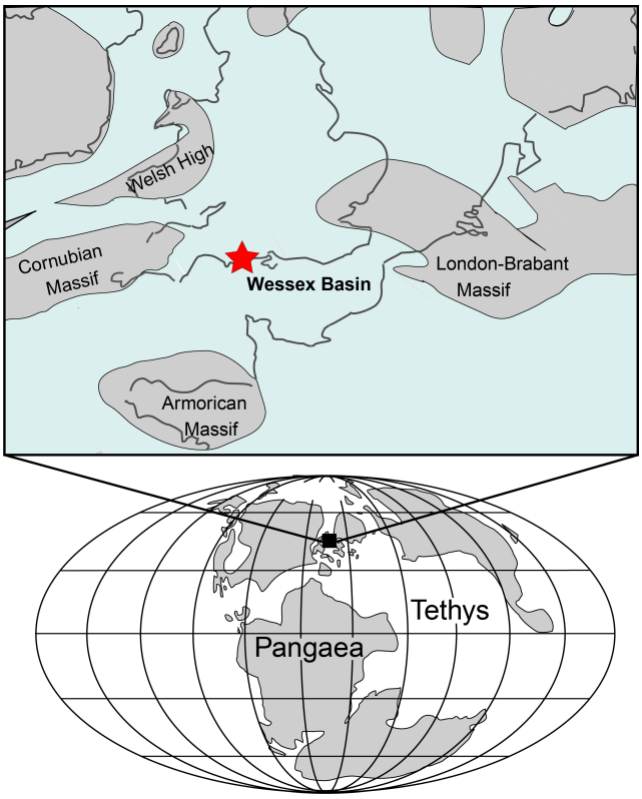

Figure 1. Paleogeographic map (Kimmeridgian) and core location. Location of the Swanworth Quarry and Metherhills boreholes in the Wessex Basin is illustrated by the red star (adapted from Williams et al., 2001).

In the absence of strong perturbations to the Hg cycle, variations in Hg_T and Hg speciation will primarily be controlled by host-phase availability, dilution by non-Hg binding fractions (carbonates) and changes in redox conditions or diagenesis (e.g., Outridge et al., 2007; Sanei et al., 2012; Frieling et al., 2023). In this study, we focused on the 113–38 meters composite depth (mcd) interval of the SQ-1 borehole (Fig. 2, 3; described by Gallois, 2000) which were deposited in the Tithonian (*ca.* 146 – 145 Ma; Hesselbo et al., 2020). The studied interval spans the entire *fittoni* and the upper parts of the *rotunda* ammonite zones and is marked by an overall regressive phase (Morgans-Bell et al., 2001). The studied succession is composed of interbedded siltstones and mudstones of variable thickness but also marked by organic-rich (bituminous) mudstone horizons at 71.45 – 72.25 mcd and 87.35 mcd and calcareous mudstones from 97.8 – 113 mcd. Based on the astronomical pacing of variations in the total organic carbon (TOC) concentrations

and borehole measurements (Huang et al., 2010), our studied section spans covers *ca.* 840 kyr and starts *ca.* 1.2 Myr younger than the material studied by Percival et al. (2015) from the same borehole (Fig. 2). Percival et al. (2015) showed that Hg and TOC varied in parallel and are reasonably well correlated for the TOC-rich lower part of the succession ($R^2 = 0.47$), resulting in mostly steady, low, Hg/TOC ratios (5 – 10 ppb/wt%); a value similar to subrecent, unpolluted, marine organic-rich sediments (e.g., Frieling et al., 2023; Leipe et al., 2013; Shen et al., 2020).

Table 1. List of Hg-species that may occur in geological sediment samples and their thermal desorption characteristics

Hg species	Approximate maximum release T (ºC)	References	Remarks
elemental Hg (Hg^0)	0 - 100	(Biester et al., 2000)	Hg^0 can occur in specific natural environments (ore-forming hydrothermal systems)
pyrite-bound Hg (Hg-FeS_2)	170	(Rumayor et al., 2016)	could be in form of HgS ((meta-) cinnabar) inclusions
HgS (metacinnabar)	190	(Rumayor et al., 2016)	common in mercury ore belts, may occur as detrital in nearby sediments
methylated Hg ($HgCH_3^+$)	200	(Saniewska & Bełdowska, 2017)	ubiquitous in (sub-)recent sediments, largely untested for rock samples (Rakociński et al., 2020)
organic-matter bound Hg	220	(Rumayor, Diaz-Somoano, et al., 2015; Saniewska & Bełdowska, 2017)	Hg in various organic compounds and products (humic acid, phytoplankton, macrophyte material)
HgSe (tiemannite)	260	(Rumayor, Lopez-Anton, et al., 2015)	Hg and Se show similar stratigraphic profiles in some sediments (e.g., Mercone et al., 1999)
HgS (cinnabar)	300	(Rumayor, Lopez-Anton, et al., 2015)	common in mercury ore belts, may occur as detrital in nearby sediments
HgO (montroydite)	470	(Biester et al., 1999; Rumayor et al., 2013)	common by-product of roasting during Hg mining, may occur as detrital in nearby sediments
$HgSO_4$ / $HgSO_4$.2HgO	580	(Biester et al., 2000; Rumayor, Lopez-Anton, et al., 2015)	$HgSO_4$ decomposes in water to $HgSO_4$.2HgO
HgFeOOH	complex	(Petranich et al., 2022)	Fe-oxyhydroxides are widely recognized as important factors in sedimentary Hg cycling (e.g., Gagnon et al., 1997)
Hg-halides (e.g. HgI_2, $HgBr_2$, Hg_2Cl_2, $HgCl_2$)	<150	(Rumayor et al., 2013; Rumayor, Diaz-Somoano, et al., 2015)	labile / water-soluble, compounds unlikely to occur in aquatic sediments

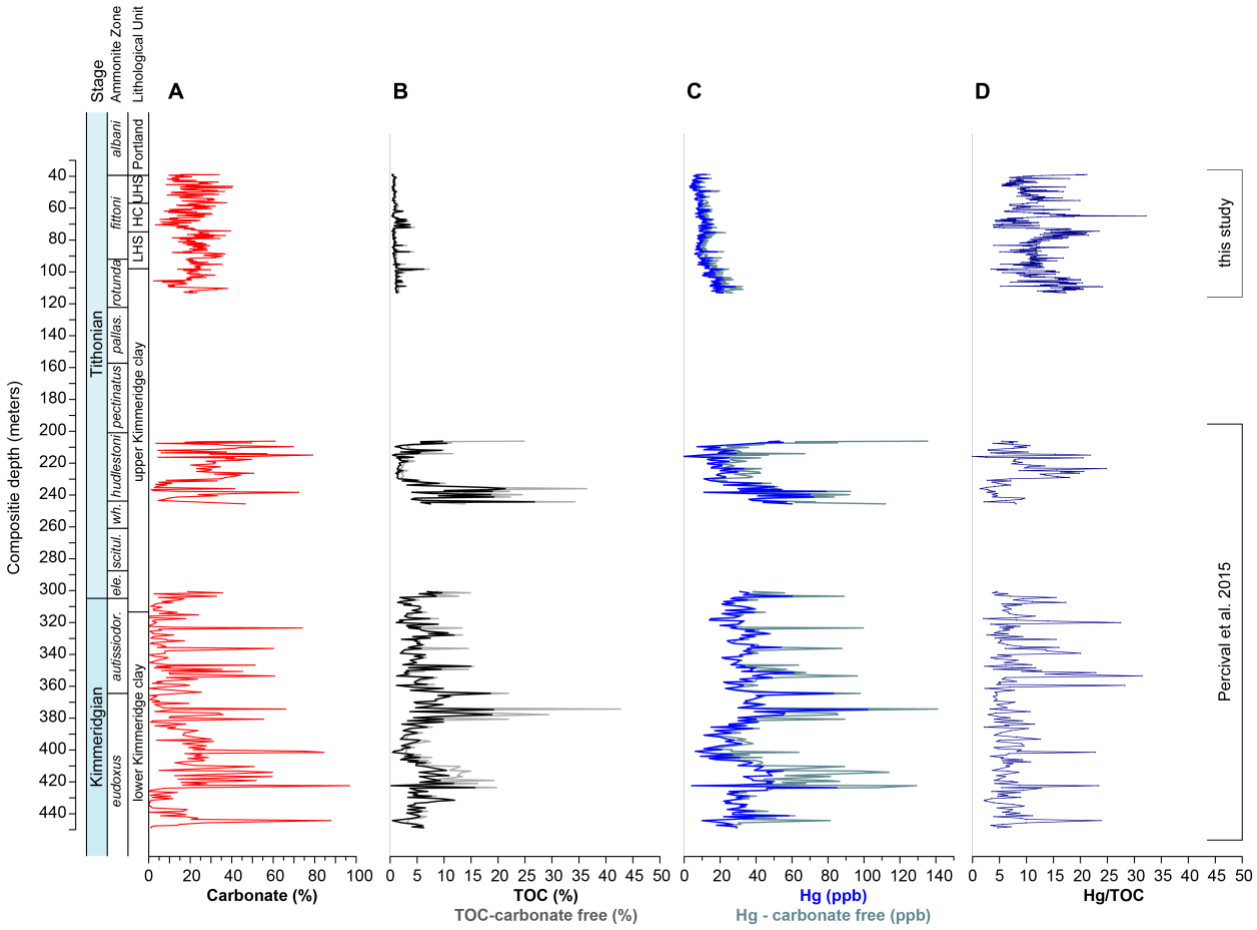

Figure 2. Stratigraphic overview for the Kimmeridge clay formation cores (Swanworth Quarry-1 and 2, and Metherhills-1). A. Carbonate percentage data. **B.** Total organic carbon percentage, and TOC on carbonate-free basis. **C.** Mercury concentration, and on carbonate-free basis. **D.** Mercury normalized to TOC. All carbonate and total organic carbon percentages were obtained from previous work (Jenkyns et al., 2001; Morgans-Bell et al., 2001) as were sedimentary mercury data for the intervals below 200 mcd (Percival et al., 2015). Abbreviated ammonite zonations: *Aulacostephanus euxodus* = *euxodus*, *A. autissiodorensis* = *autissiodor.*, *Pectinatites elegans* = *ele.*, *P. scitulus* = *scitul.*, *P. wheatleyensis* = *wh.*, *P. hudlestoni* = *hudlestoni*, *P. pectinatus* = *pectinatus*, *Pavlovia pallasioides* = *pallas.*, *Pavlovia rotunda* = *rotunda*, *Virgatopavlovia fittoni* = *fittoni*, *Progalbanites albani* = *albani*. Abbreviated lithological units: Lower Hounstout Silt = LHS, Hounstout Clay = HC, Upper Hounstout Silt = UHS, Portland Sand = Portland.

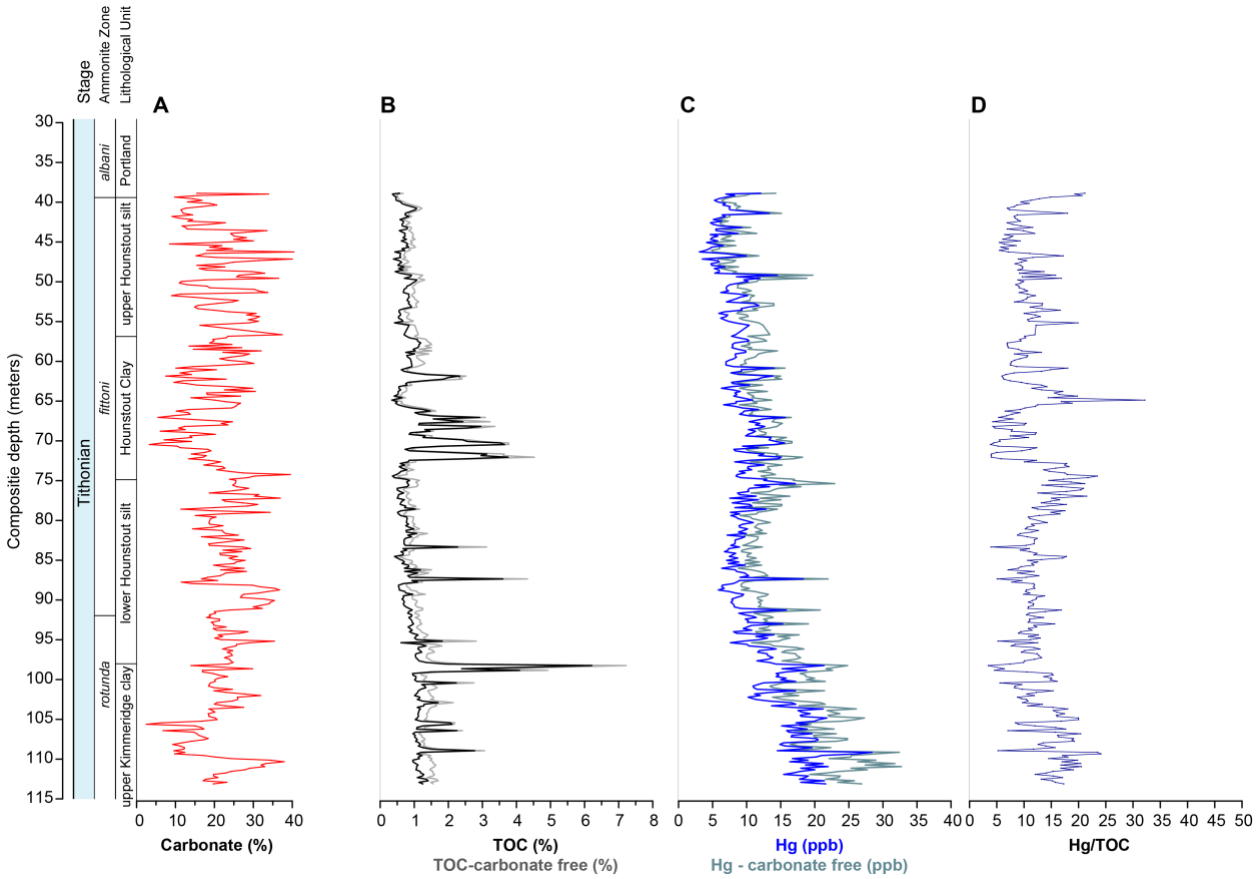

Figure 3. Stratigraphic overview for the Kimmeridge clay formation cores focused on the 30 – 115 mcd interval used in this study. A. Carbonate percentage data. **B.** Total organic carbon percentage, and TOC on carbonate-free basis. **C.** Mercury concentration, and on carbonate-free basis. **D.** Mercury normalized to TOC. Note that the x-axis scales of panels **A-C** are adjusted relative to those in Figure 2 to illustrate variability. All carbonate and total organic carbon percentages were obtained from previous work (Jenkyns et al., 2001; Morgans-Bell et al., 2001). Abbreviated ammonite zonations: *Pavlovia rotunda* = *rotunda*, *Virgatopavlovia fittoni* = *fittoni*, *Progalbanites albani* = *albani*.

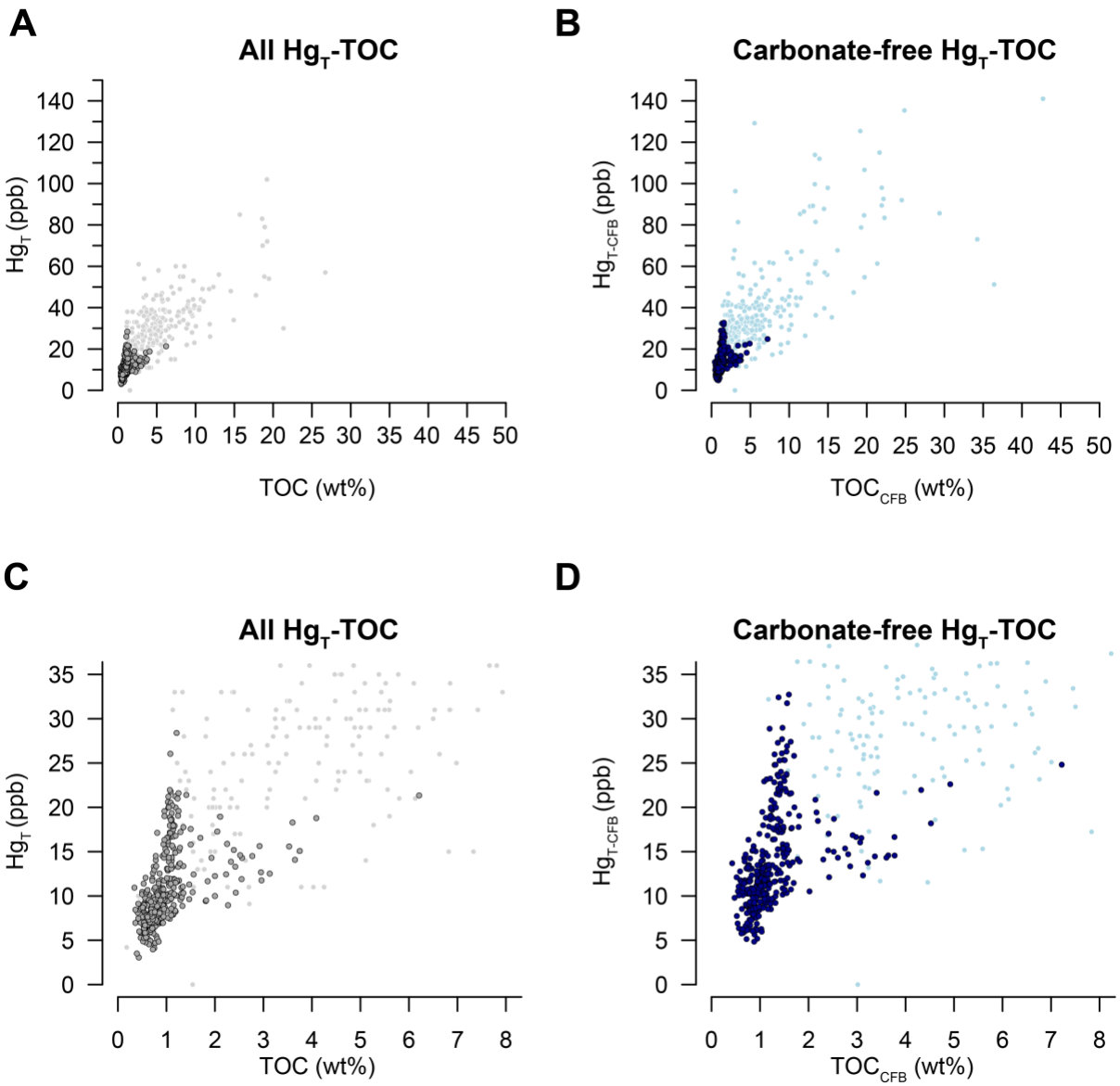

Figure 4. Mercury vs total organic carbon concentration for the combined Kimmeridge clay formation dataset. **A.** x-y plot of Hg_T and TOC, **B.** as A but on a carbonate-free basis (CFB), **C & D.** as A and B but zoomed in on the Tithonian samples. Dark colored symbols in each panel denote the Tithonian subset analyzed for this study.

2.2 Methods - total Hg measurements

Total sedimentary Hg (Hg_T) was analyzed at the University of Oxford on 200–400 mg of finely powdered rock for 363 samples using a Lumex RA-915 Portable Mercury Analyzer paired with a PYRO-915+ pyrolysis unit. Sample material was placed in a furnace at ~700 ºC, volatilizing Hg, which is then oxidized to Hg^0 in air and quantified continuously via spectral absorption, without any trapping or preconcentration. Duplicate sample analyses (n = 15) showed that typical analytical reproducibility was <10% and accuracy is *ca.* 6% based long-term observations of a high-mercury (290 ± 9 ppb) soil standard

(National Institute of Standards & Technology (NIST) 2587)(see, e.g., Frieling et al., 2023). Thermal desorption profiles were generated for a subset of 65 samples using a Lumex RA-915M, also set-up with a PYRO-915+. The Hg yield from the soil standard (NIST 2587) was routinely checked with two other sediment NIST standards (#1944, New Jersey waterway sediment, 3400±500 ppb and #2782, Industrial sludge, 1100 ± 190 ppb). Mercury is reported as sedimentary Hg concentrations (in ng g^{-1} or ppb) and normalized to weight per cent total organic carbon (Hg/TOC) (ppb/%). These NIST standard materials were also used alongside natural sediments to illustrate differential Hg desorption.

2.3 Methods - thermal desorption

Desorption profiles of natural samples (n = 65), sediment replicates with variable weights (n = 15) and standard materials (n = 30) were obtained with a Lumex RA-915M paired with a PYRO-915+ pyrolysis unit at the University of Oxford. All Hg measurements were obtained in the highest-temperature mode (Mode 1) but without 'boost', so that the temperature in the furnace remained stable throughout the analyses. The temperature of the pyrolysis chamber in this mode is specified as ~700 ºC. Samples at room temperature (20 ºC) were introduced into the furnace and rapidly heated to 700 ºC, effectively imposing a short, steep, temperature ramp. Each sample typically released Hg during 1 – 3 minutes. In addition to replicates of standard materials, two randomly chosen samples from the KCF were run in replicate (n = 5 and n = 10) to illustrate the effects of variable sample weights. To obtain consistent desorption profiles for all other sedimentary rock samples (with relatively low Hg concentrations), the weight of each sample was held constant at a weight sufficient to allow reproducibility of low-Hg samples (average 202 ± 5 mg).

The release profiles for each sample were obtained simultaneous with standard Hg_T and the detector signal at one second increments was extracted post-run from the raw time-series output (Fig. 5). As the timing and thereby the temperature ramp for each measurement needs to be identical to align the samples, we marked the 'start' of a sample measurement immediately upon inserting the sample into the furnace (although this is marked at t = 10s in terms of the sample run, see Fig. 5). The raw sample data from the entire run were subsequently extracted by using the same sample start and end point flags as recorded in the Lumex's "RAPID" software. The baseline intensity signal was calculated from two 10-second intervals before and after the sample was inserted into the furnace (Fig. 5). The baseline is subsequently subtracted from the raw detector signal to obtain the desorption profile.

After this step, the area below the intensity curve can be integrated in similar fashion as is performed via the "RAPID" software. The integrated area, which is converted to total analyzed Hg (in ng), from the offline processed data typically does not deviate more than a few tenths of % from the standard "RAPID"-estimates and can be converted to Hg release and concentration with a standard-calibrated

detector sensitivity and the sample mass. The desorption profile data for each sample is provided as a separate file, as are example files and R-code to extract the profiles.

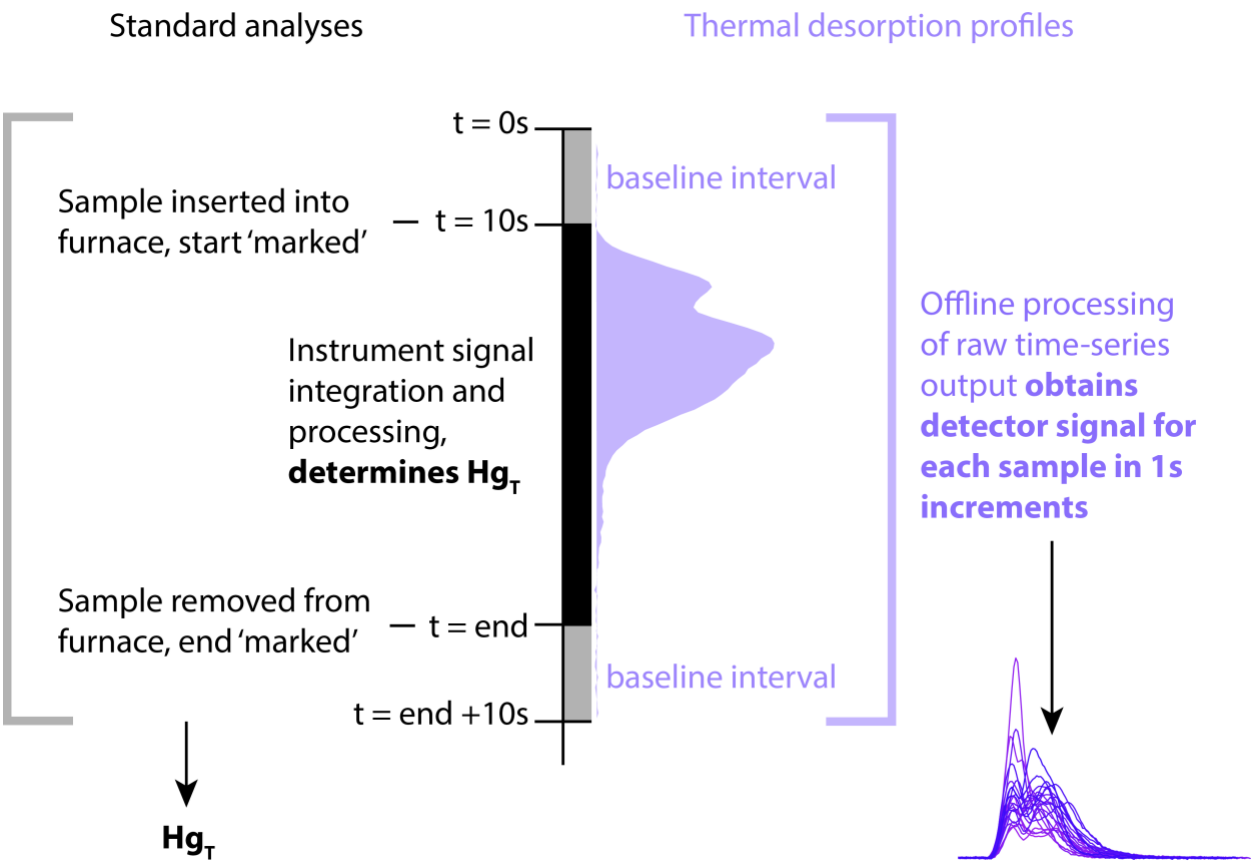

Figure 5. Schematic overview of simultaneous acquisition of Hg_T and thermal desorption profiles for each sample.

3 Results & Discussion

3.1 Analytical considerations and limits

To examine the profiles, we calculated the signal intensity in Hg mass released per second for each gram of the (total) sample material (in ng g^{-1} s^{-1}) (e.g., Fig. 6). The absolute release intensities (in ng g^{-1} s^{-1}) are suitable to assess at which stage most Hg is released from the sample material and to directly examine which fractions may be enriched within specific samples. Alternatively, an area-normalized signal (*i.e.* a fraction of total Hg release, Fig. 7E, F) can facilitate direct comparison of profiles from samples with (strongly) varying concentrations, providing insight into changes in proportional importance of Hg release phases.

Analytical noise typically does not play a large role in the reproducibility of total Hg measurements; even at low Hg concentrations and sample weight the total Hg released from geological samples is usually well above the total manufacturer-specified detection limit (~0.1 ng Hg). However, it is a more important consideration for desorption profiles as we used partial signals and corresponding lower overall signal and intensity for individual 1-second increments. The typical standard deviation (noise) on the instrument's detector signal was observed to be of the order of 0.8 units, which converts to ~0.001 ng Hg s^{-1}. Even natural samples with low Hg concentrations (~15 ppb) and relatively small sample weights (<100 mg) yield signal intensities at least an order of magnitude above this level (Fig. 6D, E).

For lower concentrations and more complex release patterns in natural samples (Fig. 6), we tested the impact of analyzed sample mass. We found that variable weights impact Hg release profiles and sample mass can appreciably influence the release fraction (Fig. 6F). This is likely due to thermal inertia of the larger sample masses (>50 mg) combined with relatively higher abundance of high-temperature Hg phases compared to the standard materials. It is therefore recommended that sample weights are kept similar to compare samples, certainly when low-Hg samples (<10 ppb) are included in the analytical run as they often require larger sample masses (> 100 mg) to reliably measure. Weight effects in standard materials were insignificant, because the sample weights are typically smaller (<50 mg) and Hg releases at low temperature resulting in generally narrower peaks (Fig. 5).

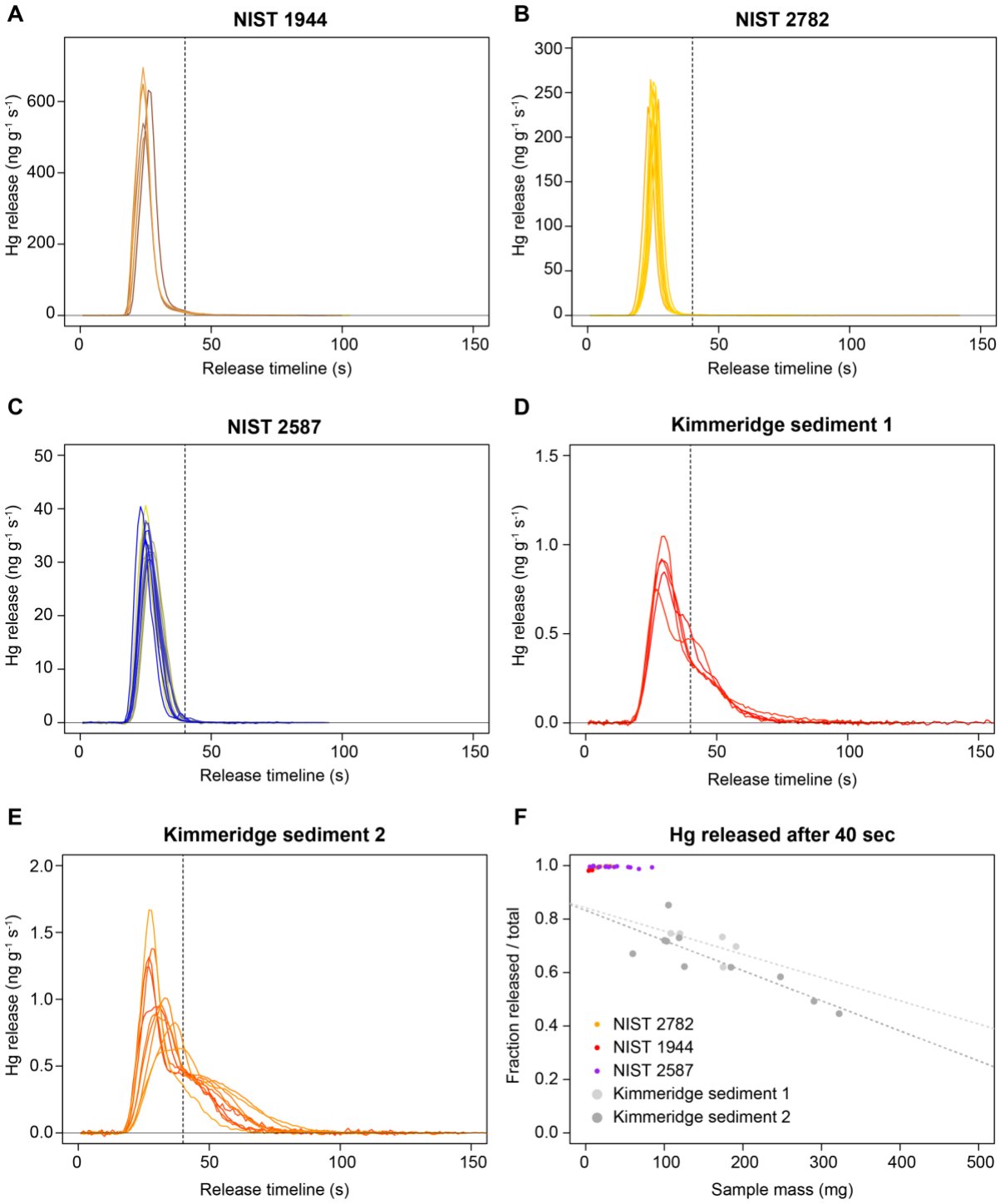

Figure 6. Example release profiles for Hg and influence of sample mass on release. A. NIST 1944 (New Jersey waterway sediment, ca. 3.4 ± 0.5 ppm). **B.** NIST 2782 (Industrial sludge, ca. 1.1 ± 0.19 ppm Hg). **C.** NIST 2587 (Paint-contaminated soil, ca. 290 ± 9 ppb). **D and E.** Two low-Hg samples (16.6 ± 0.2 ppb, n = 5 and 21.2 ± 0.6 ppb, n = 10) from the Kimmeridge clay formation. For A-E, mercury release is shown as ng per gram of sample material per second (ng g^{-1} s^{-1}). **F.** Mercury released as fraction of total Hg before 40 seconds in the analysis timeline (dashed

line in panels A-E) *vs* sample mass in mg. Kimmeridge sediment 2 shows significantly reduced release with increasing mass ($p \sim 0.002$).

Table 2. Mercury (in ppb) and total organic carbon (in weight percent) data and correlation for the entire succession and by lithology. Ranges for values are given in 16^{th}-84^{th} percentiles; ±1 standard deviation equivalent.

Dataset	Data (n)	Hg_T (16^{th}-84^{th} percentile)	TOC (16^{th}-84^{th} percentile)	Correlation (R^2)	p-value
All KCF data	604	7.9-32	0.7-5.2	0.657	<0.001
Percival et al. (2015)	241	20-43	2.0-8.6	0.468	<0.001
This study	**363**	**7-15.5**	**0.6-1.2**	**0.215**	**<0.001**
Mudstones	138	7-11.9	0.7-1.2	0.232	<0.001
Siltstones	127	6.2-10.2	0.5-0.8	0.131	<0.001
Carbonates	88	11.5-20	1-1.4	0.036	0.078
Organic-rich mudstones	10	12.1-15.4	2.6-3.6	0.424	0.041
All desorption samples	66	8.9-18.3	0.7-1.3	0.186	<0.001

Table 3. Thermal desorption profile-informed mercury release, fraction of Hg (in ppb) in total organic carbon (in weight percent)

Dataset	Data (n)	Hg in first phase (0-39 seconds) (16^{th}-84^{th} percentile)	TOC (16^{th}-84^{th} percentile)	Correlation (R^2)	p-value	Hg_T-original Correlation (R^2)	p-value
All desorption samples	66	3.8-9.5	0.7-1.3	0.59	<0.001	0.186	<0.001
Mudstones	22	4.1-8.3	0.7-1.2	0.35	0.002	0.17	0.032
Siltstones	18	3-7.8	0.5-0.8	0	0.344	0	0.367
Carbonate mudstones	22	5.2-10.4	1-1.4	0.64	<0.001	0.015	0.262
Organic-rich mudstones	4	9.9-12.7	2.6-3.6	0.86	0.048	0.61	0.14

3.2 General observations on natural samples

Mercury concentrations are low (7 – 15.5 ppb) for the section studied here, and always well below the shale average (~63 ppb) of Grasby et al. (2019), although it should be noted that we focused on a period without known LIP volcanism unlike most of the works included in their compilation. Total organic carbon values are typically between 0.6 and 1.2 % for the same samples, resulting in an average Hg_T/TOC of 7.9–16.6 ppb / %. The Hg_T concentration of the section analyzed for this study is lower than that of the interval analyzed by Percival et al. (2015), as is the TOC (Table 1) but the Hg/TOC is higher (7.9–16.6 compared

to 4.0 – 10.7 ppb / %) (Fig. 2D). In general, a higher Hg/host-phase at lower host-phase abundance and *vice versa* (Fig. 4C) are indicative of non-linearity in the Hg-host-phase relation, which has been observed previously (Fendley et al., in press; Frieling et al., 2023; Grasby et al., 2019). Besides analytical limitations on the host-phase measurements (Grasby et al., 2019), these non-linearities can stem from oxidation effects on host-phase abundance on the low-end and evasion of Hg or dilution by the host-phase at the high-end (Fendley et al., in press; Frieling et al., 2023). Regardless, the Hg_T-TOC correlation for the entire succession (combined data from Percival et al. 2015 and our study, n = 604, Table 1) is strong (R^2 ~0.66) and thus, overall, TOC variability appears most closely aligned with Hg_T variability. Morgans-Bell et al. (2001) estimated inorganic carbon (TIC) content from the difference between total carbon (untreated material) and TOC (acid-treated, decarbonated) and assuming all inorganic carbon resides in $CaCO_3$, multiplied TIC by 8.333 to obtain carbonate content. Carbonate shows a weak but significant negative correlation with both TOC and Hg, which likely indicates a degree of carbonate dilution of these phases (Fendley et al., in press). Carbonates in the KCF comprise a wide range of both primary and secondary phases (calcite, dolomite, siderite; Morgans-Bell et al., 2001; Scotchman, 1991) that are likely to have a diluting effect on non-carbonate compounds. We therefore also show the carbonate-free fractions (Figs. 2 B,C; 3 B,C; 4 B,D) but note that this does not affect Hg/TOC as both are generally assumed to be exclusively hosted in the non-carbonate fraction.

When the data from the succession is examined in subsections and specific lithologies, we find that the Hg_T-TOC correlation is much weaker for the interval analyzed for this study (R^2 = 0.22, n = 363) than for the entire KCF succession. Although the correlation for a small subset of our samples characterized as organic-rich (bituminous) mudstones is somewhat stronger (R^2 = 0.42, n = 10), the same cannot be said for siltstone (R^2 = 0.13) and carbonate-rich mudstone lithologies (R^2 = 0.04) (Table 2).

3.3 Insights from thermal desorption profiles

Thermal desorption profiles (TDPs) were analyzed for a representative subset of 65 samples from the upper interval (113 – 30 m) (Figs. 7 – 11). We employ TDPs to test whether the poorer correlation in Hg-TOC in the studied interval is due to occurrence of multiple Hg-species. First, the thermal desorption profiles are separated by lithology and visually examined (Fig. 7). The profiles show a degree of systematic behavior between the various lithologies, strongly suggesting multiple phases of Hg release in most samples, although the organic-rich mudstones are typically dominated by a single phase. Inspection of individual profiles in the mud- and siltstones and carbonate mudstones indicated that many have two separate maxima, i.e., multiple (double) peaks. The first peak, with a maximum at around 30 seconds after start of the run, often dominates in amplitude whereas the second peak is more protracted with maximum release around *ca.* 45 seconds. When TDPs from different lithologies are compared quantitatively, the

organic-carbon rich mudstones have the most straightforward release profile, as most Hg is released in a single dominant peak that centers around ~30s and >90% of the total Hg is released before 50s. For the carbonate-mudstones and mudstone lithologies late-stage Hg release (>50s) is proportionally much more important (average ~30%) and the siltstones are in between (~25% release after 50s). There is however also significant variability within these lithological groups, which indicates that the lithology is not the only factor in shaping the release profiles.

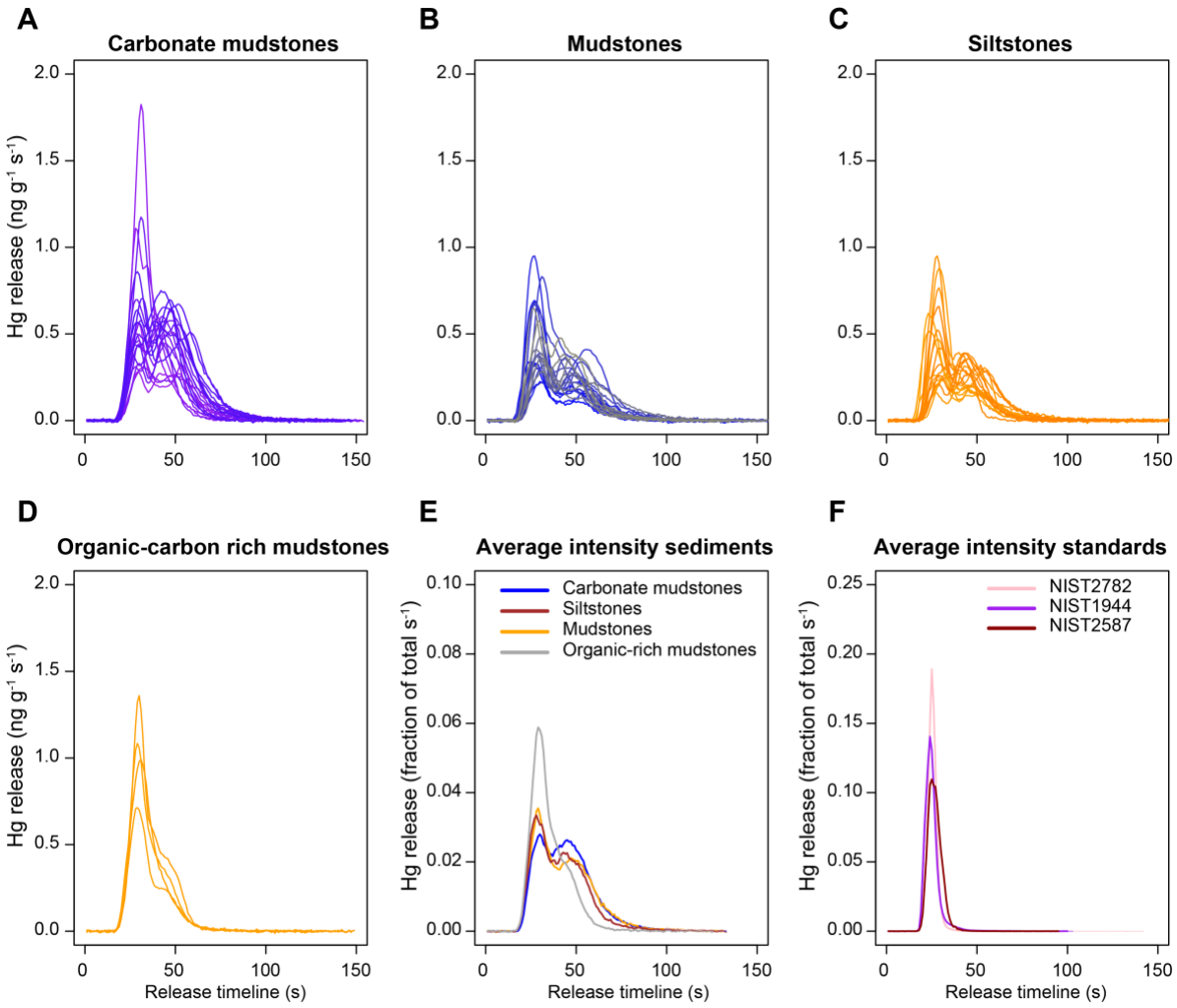

Figure 7. Thermal desorption profiles for natural samples and standard aliquots analyzed in this study. The sample is inserted into the furnace at t = 10s (t_0 - t_{10} is used for the baseline) and the area below the curves is integrated to calculate the total and phase-specific Hg concentration (see also Fig. 5). **A.** Release profiles for each of the carbonate mudstone samples. **B.** As panel A for mudstones. **C.** As panel A for siltstones. **D.** As panel A for organic-rich (bituminous) mudstones. **E.** Average release intensity for lithologies shown in A-D, normalized to total Hg release for each sample. **F.** As panel E but for the NIST reference sediment replicate analyses shown in Figure 6.

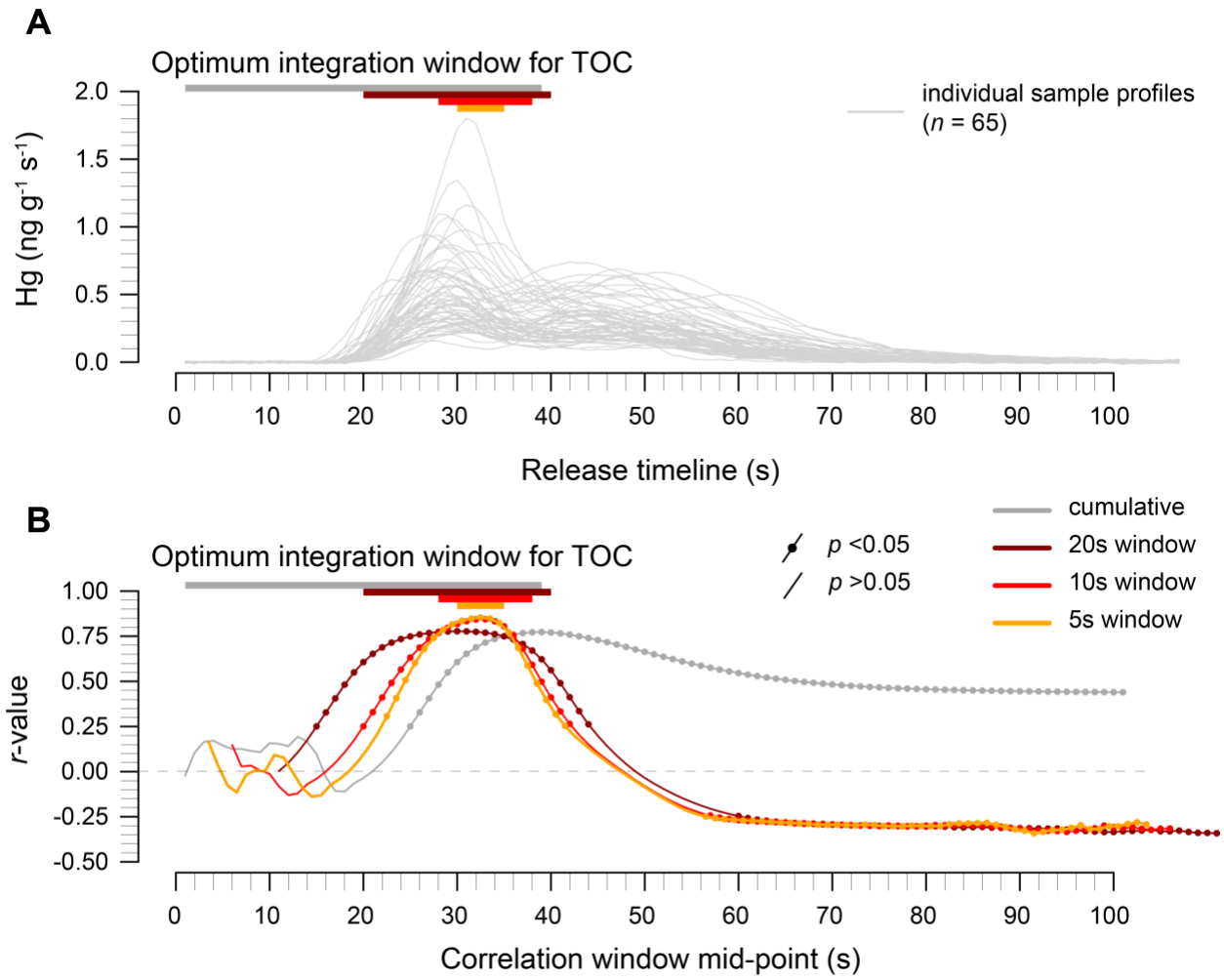

Figure 8. Mercury desorption intensity per gram of sample material (in ng g^{-1} s^{-1}) and correlation to the total organic carbon concentration, across all 65 samples. A. Position of the optimum integration windows (as determined via correlations shown in panel B) relative to desorption profiles of the Kimmeridge clay formation samples. **B.** Mercury release for rolling windows shifted at 1-second increments (i.e. 1 – 6 seconds, then 2 – 7 seconds) was integrated and then correlated to TOC. Windows cover intervals of 5, 10 and 20-seconds. The cumulative integration grows by 1-second from t_1-t_2 to t_1-t_3, t_1-t_4 etc., in which the final step t_1-t_{end} is equivalent to standard Hg_T/TOC. Note the significant negative correlation coefficients for $>t_{60}$ identified in the 5, 10 and 20 second intervals. Optimal integration for the 20s, 10s and 5s windows are found at t_{20-40}, t_{28-38} and t_{30-35}, defined as the position of maximum *r*-values. For the cumulative integration, the optimum window is defined as the interval up to and including the highest *r*-value (t_1-$_{39}$).

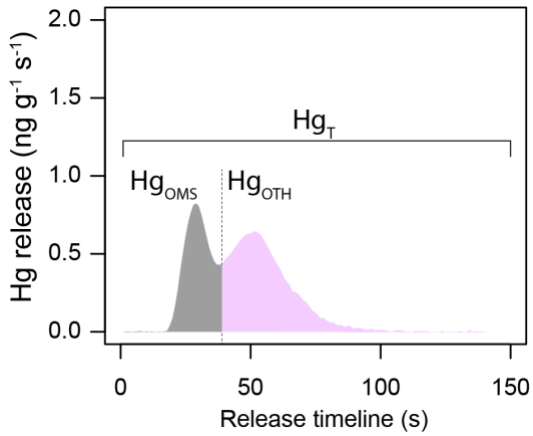

Figure 9. Example of Hg release phases within a sample divided based on the optimum correlation to TOC (cumulative, Figure 8). Dashed line signifies the cut-off between organic-matter and OM-associated sulfur bound Hg (Hg_{OMS}) and other Hg release phases (Hg_{OTH}) (here 39 seconds) (see also §3.4). Total Hg (Hg_T) is equal to the sum of Hg_{OMS} and Hg_{OTH}.

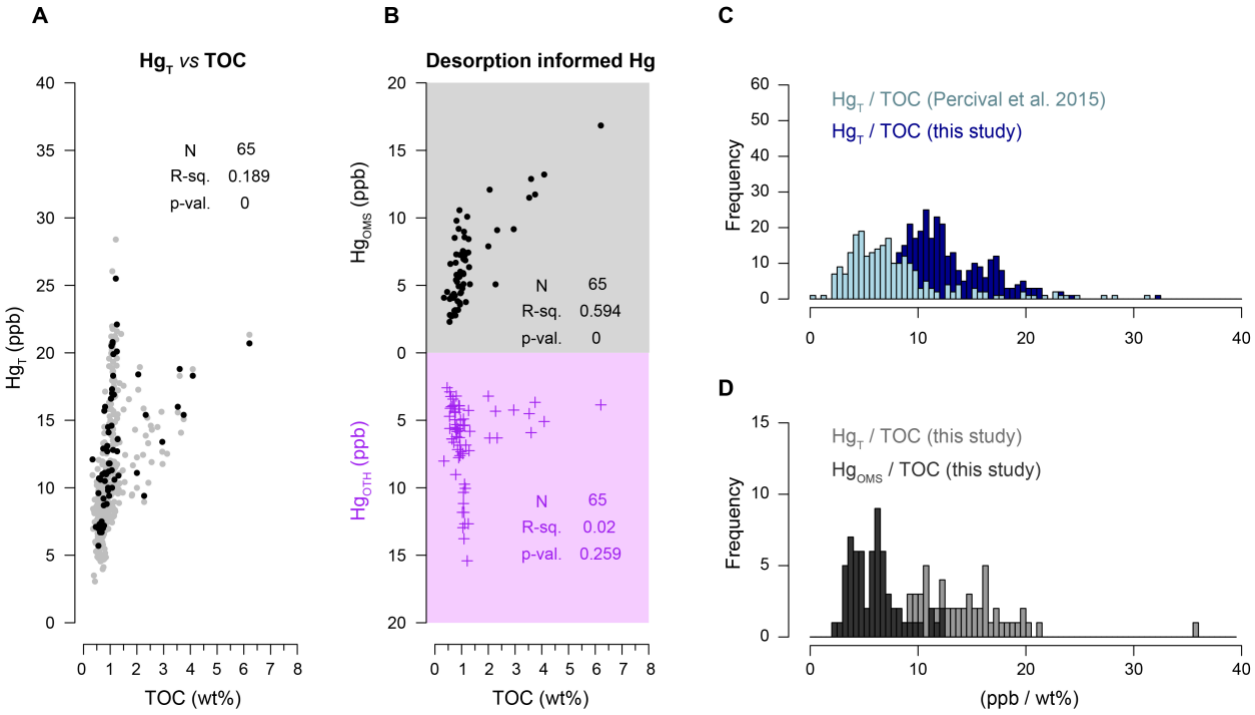

Figure 10. Desorption characteristics for the Tithonian samples. A. All samples analyzed for this study (grey) and the representative subset analyzed for thermal desorption profiles (black) with weak overall correlation. **B.** Cumulative mercury release before 39 seconds (Hg_{OMS}, top, black) and after 39 seconds (Hg_{OTH}, bottom, purple, note inverted y-axis scale) for individual samples. **C.** Frequency histogram of Hg_T normalized to TOC for all samples analyzed in this study compared to the organic-rich lower Kimmeridge clay formation samples (Percival et al., 2015). **D.** Hg_{OMS}/TOC and Hg_T/TOC of the TDP-informed samples.

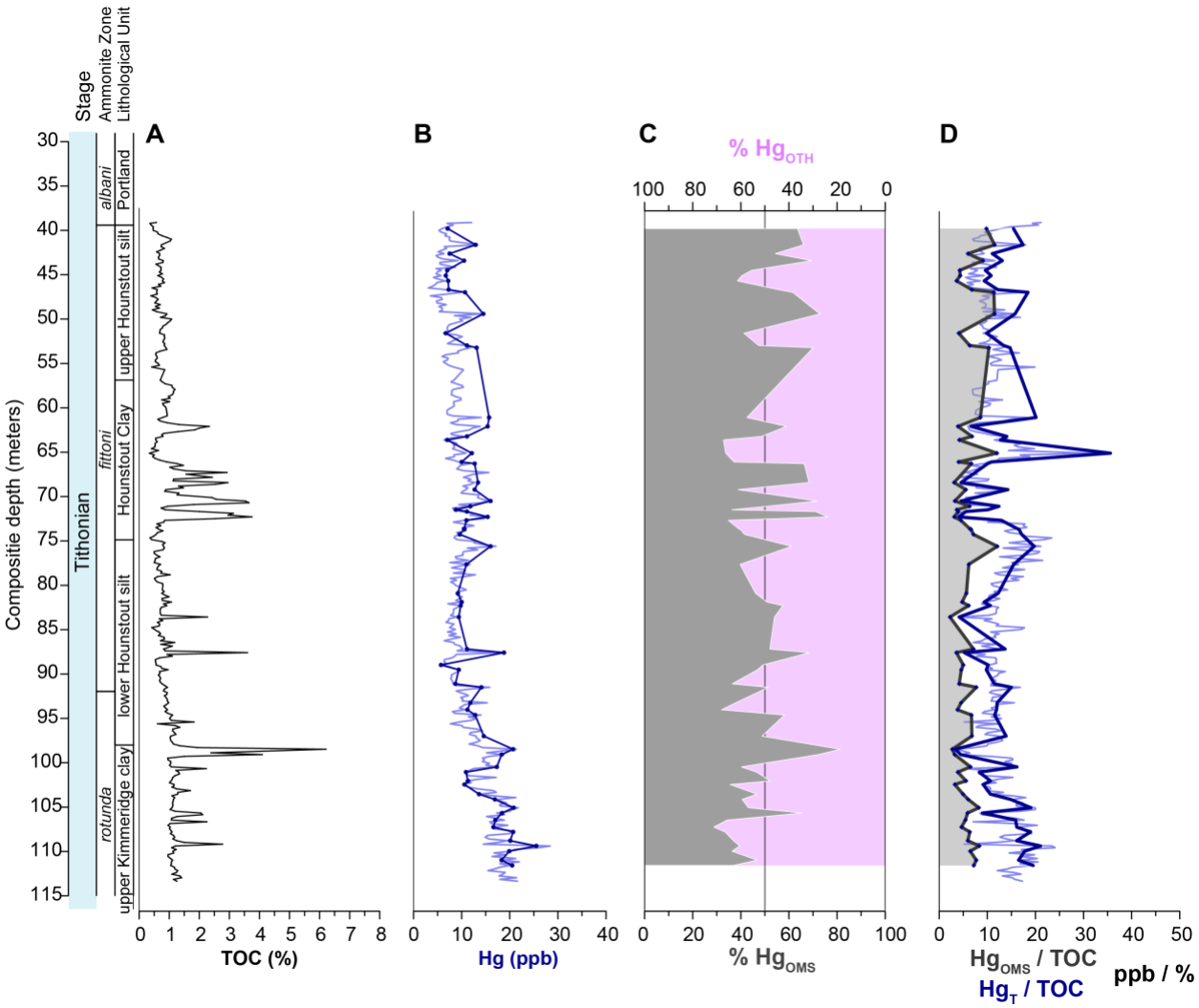

Figure 11. Desorption informed Hg data in stratigraphic context. A. Total organic carbon concentration. **B.** Hg concentration (light blue = all samples, blue line = desorption samples). **C.** Relative abundance of Hg_{OMS} and Hg_{OTH} for each desorption sample (for example, see Figure 9). **D.** Hg_{OMS} normalized to TOC (shaded area, thick black line) and Hg_T normalized to TOC (thin blue line = all samples, thick blue line = desorption samples). Abbreviated ammonite zonations: *Pavlovia rotunda* = *rotunda*, *Virgatopavlovia fittoni* = *fittoni*, *Progalbanites albani* = *albani*.

3.4 Evidence for Hg species, host-phases and relation to thermal desorption peaks

The evidence for multiple release peaks during heating that signals the presence of multiple Hg species (Fig. 8) prompts us to consider the host-phase relation for the individual peaks. We therefore examine the release intensity per gram of sample material for specific intervals of the TDPs. In Figure 8, two approaches are shown. First, the cumulative release up to a certain point in the TDP is compared to the total TOC measured in each sample, which shows a distinct peak in correlation-strength (r ~+0.75, R^2 ~0.6) at 39s. After this point, the correlation strength with TOC decreases. Second, we examine Hg release over

5, 10 and 20-second intervals shifting the window by 1-second increments over the duration of the sample run and correlate it with TOC. This confirms that the interval from 20 to 40s has the strongest positive correlation to TOC ($r > +0.75$, $R^2 > 0.6$), as also indicated by the cumulative release up to 39s. When focused into shorter intervals, we find that the maximum strength of the correlation is further increased to r values around +0.85 ($R^2 > 0.7$) in the intervals 28–38s and 30–35s, suggesting >70% of variance in Hg released in this TDP peak can be explained by TOC variability. This remarkable difference with Hg_T/TOC ($r \sim +0.44$, $R^2 \sim 0.18$, $n = 65$, Table 3) appears to be due to a secondary peak in Hg release, beyond 40s into the sample analyses (Fig. 7). For Hg released >50s, the correlation for Hg-TOC is weakly ($r \sim -0.3$, $R^2 \sim 0.1$) but significantly ($p < 0.05$) negative (Fig. 8B).

Although a correlation with TOC may not directly signal that the first Hg peak in the TDPs relates to OM-bound Hg in the TDPs, multiple lines of evidence suggest it is indeed most likely OM or an OM-associated host-phase being desorbed at this stage. First, all analyzed samples contain this phase, and as Hg is presumed (dominantly) OM-bound upon deposition we would thus expect such a phase to be omnipresent unless all OM is broken down (oxidized) after deposition, which is not the case here as TOC rarely drops below 0.5%. Second, for the organic-rich (bituminous) mudstone, where the TOC is high, Hg release is focused as a single peak and the Hg_T-TOC relation is comparatively strong ($R^2 = 0.42$). This suggests more closely coupled Hg_T-TOC behavior, as was found for the more organic-rich KCF interval analyzed by Percival et al. (2015). Finally, previous Hg speciation and thermal desorption studies that have shown that OM-bound Hg in natural sediments is usually the phase from which Hg desorbs at the lowest temperature (Biester & Scholz, 1997; Rumayor, Diaz-Somoano, et al., 2015; Saniewska & Bełdowska, 2017). Other Hg-species (e.g., elemental Hg, Hg-chlorides and Hg-bromides) with lower desorption temperatures are considered more labile and their (abundant) occurrence appears limited to ore materials or polluted sediments (Table 1)(Rumayor et al., 2017). The KCF in places has abundant pyrite (Matthews et al., 2004; Morgans-Bell et al., 2001) and is notable for sulfurization of OM (van Kaam-Peters et al., 1998); when considering OM-bound Hg release, we therefore also consider that a portion of this Hg may in fact be associated with organic sulfur or present as inclusions in (framboidal) pyrite or metacinnabar (black HgS). These Hg species can (appear to) be coupled and correlate with TOC in sediments as they are either directly associated with OM and OM-breakdown processes (Berner, 1982, 1984; Raven et al., 2023; Werne et al., 2003) or preferentially form in presence of OM (such as HgS, e.g. Pham et al., 2014). This connection implies that the controlling factor for the sedimentary abundance of these phases during deposition might have been organic-matter flux, so that even if other chemical species (e.g., sulfides) now bind Hg, the abundance of these phases may still link to OM-drawdown. We hereafter refer to the first release phase as organic-matter and organic-matter associated sulfur Hg (Hg_{OMS}) and the secondary release as 'other' Hg species (Hg_{OTH}).

522

523 ### 3.5 Other mercury release phases

524 The later peaks represent Hg species with higher desorption temperatures. This higher-temperature
525 release may relate to a range of chemical species, of which sulfides (cinnabar, HgS) are typically considered
526 as important host-phases for geological samples. For example, the various studies of reference compounds
527 (Table 1) show that red HgS (cinnabar) has higher desorption temperatures and broader peaks than OM-
528 bound Hg, which may contribute to the secondary peak in our samples. However, some caution is warranted
529 as the potential diversity in sedimentary Hg-S species (Table 1) poses a major challenge; Hg may be
530 associated with sulfur via an OM-associated sulfur fraction (see also §3.4), but also various sulfides and
531 sulfates. This implies that it is not straightforward to examine the Hg-S relation in low-Hg sediments in
532 detail with any of the currently available statistical or analytical (§1.2) techniques. Besides sulfur-minerals
533 it is also conceivable that the Hg is present as, for example, Hg-oxide (HgO; montroydite), Hg-selenide
534 (HgSe; tiemannite) or Hg-sulfate ($HgSO_4$) although reports of their occurrence in unpolluted sediments are
535 limited and some of these Hg-species are generally considered rare in nature (e.g., HgO; Biester et al., 1999)
536 or unstable as they are easily dissolved or decompose in water (e.g., $HgSO_4$; Haynes, 2014). Lastly, the
537 late-stage Hg release may represent a Hg fraction locked in more refractory mineral grains, which may
538 include pyrite or other metal sulfides (e.g., PbS; galena, ZnS; sphalerite, HgS; cinnabar) but also silicates
539 or diagenetic carbonates. At the concentrations (< 10 ppb Hg) analyzed in this study, resolving and
540 quantifying which phases are present besides Hg_{OMS} will be limited by our ability to directly measure these
541 phases or locate the (rare) minerals that contain them via element mapping. To summarize, while the TDPs
542 have limitations in identifying host-phases beyond OMS (if rapidly heated), we can be reasonably confident
543 that Hg_{OMS} can be separated from other, more temperature-resistant Hg-species.

544

545 ### 3.6 Implications for Hg normalization

546 The desorption profiles and optimal correlation window for the Hg release in the individual phases
547 in our samples revealed that in approximately half the samples (35 out of 65), this first release phase
548 (Hg_{OMS}) is not dominant (Hg_{OMS} is <50% of Hg_T) (Fig. 11C). As Hg_{OTH} is roughly equally important as
549 OM-associated Hg on a succession-level but strongly varies in proportion from sample to sample (Fig. 11C,
550 D), these data show clear conflict with the common assumption that sedimentary Hg is hosted by a single
551 dominant phase. Though the first phase correlates well with TOC, normalization of Hg_T to TOC therefore
552 cannot be justified for these samples.

553 When following a traditional approach to remove enhanced Hg sequestration by OM, the strong
554 positive correlation found for the entire succession between Hg_T and TOC (R^2 = 0.66), might support the
555 normalization of Hg_T by TOC. Although much weaker, a correlation remains for the Tithonian subsection

analyzed here (R^2 = 0.2) which might be used to support a similar normalization approach. However, the TDP analyses show that the OM-associated Hg cannot be demonstrated to dominate in many samples, and that the fractional dominance of Hg_{OMS} is not confined to specific sequential sample sets or portions of the succession. Thus the simple Hg_T/TOC approach would introduce variability through the section and inflate Hg_T/TOC for all samples but to a variable extent. As multiple release phases are present in most samples, the same would likely apply to any other Hg_T host-phase normalization. As all samples where Hg_{OTH} dominates Hg_T are at relatively low TOC concentrations, proportional differences between Hg_{OMS} and Hg_{OTH} in samples here may also impact assessment of linearity of Hg_T-TOC. In this case, the secondary phase appears to anticorrelate with TOC (Fig. 8B), which further complicates interpretation of a TOC-normalized Hg_T signal.

Aside from the TDP characteristics and other techniques that resolve Hg speciation there is no obvious way to tell the dominant Hg species or host-phase at a sample-level; the samples where Hg_{OTH} dominates are within the normal TOC range for this part of the succession and appear randomly distributed throughout (Fig. 10, 11). These samples also would not be discarded because of low host-phase abundance or analytical limitations (TOC ranges from ~0.5-1.5%) and neither do their Hg_T concentrations differ from samples for which Hg_{OMS} dominates Hg_T. The lithology of the samples may have some impact as the frequency of samples where Hg_{OMS} is not dominant is highest in the carbonate mudstones. Nevertheless, the degree of dominance of Hg_{OMS} impacts Hg_T/TOC highlighting the advantage of separating the Hg_{OMS} and Hg_{OTH} phases. A greater proportion of Hg_{OTH} correlates to higher Hg_T/TOC. When only the first phase is normalized to TOC (Hg_{OMS}/TOC) values of all samples approach the Hg_T/TOC values of the more organic-rich mudstones and the organic-rich lower parts of the KCF (Fig. 10D).

If OM burial was the primary driver of Hg sequestration and abundance in our succession, the variability in TDPs for the more organic-lean samples may reflect Hg-speciation changes during syn- or post-depositional processes. Mercury speciation changes in sediments may not be uncommon as, for example, Hg enrichment in diagenetic pyrite has been documented in the geological record (Shen et al., 2019; Z. Wang et al., 2020). Here, the occurrence and frequency of multiple phases in carbonate mudstone lithologies is noteworthy. The processes driving carbonate dissolution and (authigenic) precipitation in the KCF and in general are closely linked to OM breakdown (Irwin, 1980; Irwin et al., 1977; Scotchman, 1991), which generates dissolved inorganic carbon that can be reprecipitated with free metal ions (of Ca, Mg, Mn, Fe). If Hg is released during OM breakdown, which may have substantially and variably affected parts of the KCF (e.g., Kodrans-Nsiah et al., 2009), Hg may relocate into a secondary phase. Any diagenetic effect that affects either the host-phase or Hg warrants careful consideration as the potential for relocation implies Hg may (appear to) have been concentrated in certain stratigraphic levels. Such effects may be of a similar magnitude as is associated with some perturbations proposed to be volcanic in origin (Frieling et al., 2023;

Mercone et al., 1999; Shen et al., 2019). As mentioned previously (§3.5) it is also conceivable that Hg is 'locked' in (non-sulfide) mineral grains; which may be facilitated by, for example, sediment incorporation into authigenic carbonates and/or absorption into these phases (cf. Biester et al., 1999). We therefore emphasize that, while we demonstrate that the Hg_{OMS} phase is of variable importance in these sedimentary rocks at the time of our analyses, Hg drawdown may have been facilitated by OM-fluxes at the time of deposition (146 – 145 Myr ago).

3.7 Mercury speciation and enhanced Hg loading

Without the use of TDPs or other sample-level Hg speciation, we follow previous studies (Fendley et al., in press; Frieling et al., 2024; Percival et al., 2021) in their interpretation and recommendation that anomalous Hg loading should still be evidenced by at least two of the following: (1) exceptional Hg concentrations, (2) exceptional normalized or excess Hg, when appropriately corrected for host-phase effects and, ideally, (3) exceptional Hg mass accumulation rates.

The simple Hg speciation approach used here is principally a test to what extent Hg_T is impacted by multiple Hg species or host-phases and whether single-phase normalization of Hg is justified. The key strength of the approach is in pinpointing which samples may be false positives or false negatives due to Hg normalization to an unrelated host-phase. Such constraints are particularly relevant in the normalized Hg_T data that are ubiquitously used in efforts to trace LIP-volcanic activity in ancient rocks that encompass large-scale environmental changes. This ranges from extreme end-members such as enhanced Hg release from specific fractions in discrete stratigraphic levels (e.g., diagenetic pyrite)(Gong et al., 2017; Shen et al., 2019), which may have focused Hg, to subtler variations between samples such as observed in our Tithonian sample set.

The Hg TDPs measured on the KCF material show a substantial degree of variability in Hg speciation that is not simple to predict based on available parameters (lithology, carbonate, TOC). Such complexity in Hg speciation is not unexpected as data from (sub-)recent sediments shows that Hg speciation can strongly vary through time and space. Moreover, our data indicate Hg speciation changes may be of complex diagenetic (post-depositional) or other (syn-depositional) environmental origin, underlining the value of acquiring Hg speciation data as a starting point for further study of the origin of the Hg_T and Hg speciation signal in the sediments.

Sedimentary Hg speciation impacts our ability to infer paleovolcanic activity as the use of Hg as a proxy for LIP activity strongly depends on detection of anomalous Hg loading through means of host-phase normalization, determination of statistical outliers or (multivariate) correspondence analyses (Fendley et al., in press; Sanei et al., 2012; Kovács et al., 2024). The key assumptions (linear, predictable, single-host-phase Hg) that (implicitly) underlie all these methods have so far lacked independent validation in the form

of sample-level constraints on Hg speciation. Qualitative and quantitative information on Hg speciation, such as through TDPs, provides a means to better guide the use of these techniques and to test whether the key assumptions to use them are justified. As a theorical example, we would recommend cautious interpretation of samples with both strongly elevated (normalized) Hg and different Hg speciation compared to surrounding samples, as these may have a greater likelihood of being 'false positives'. On the other hand, any elevated Hg loading that coincides with a peak in the host-phase proxy (TOC, TS or clays) would be easily missed by aggressive (linear) normalization (heightened chance of false negatives). If such samples are not characterized by a change in Hg speciation, those Hg peaks may require further investigation as to why Hg has accumulated.

3.8 Method applicability & adaptability

The approach used for this study can be applied directly with Lumex Instruments RA-915M (used here) and the RA-915Lab, with or without auto-sampler, as it is built around the data generated and output from these instruments' software. The main advantage of continuous-flow and continuous Hg recording is that the signal does not require further processing or (pre-)concentration that may impact recovery when analysing thermal desorption (see also other studies using a Lumex RA-915, e.g., Rumayor, Lopez-Anton, et al., 2015). However, for pyrolysis based direct mercury analyzers with trapping (gold amalgamation), a similar result may be obtained through (stepped) temperature ramping of single samples or analyzing multiple aliquots of the same sample at different temperatures to obtain a thermal release-sequence (cf. Rumayor et al., 2015; Saniewska and Bełdowska, 2017; Bełdowska et al., 2018). If the details of Hg speciation in geological samples become critical to constrain, more laborious and specialized but potentially also more accurate Hg speciation methods such as element mapping, mineral identification or sequential extraction of Hg phases (§1.2) can be used alongside the aforementioned pyrolysis-based methods to resolve the exact Hg containing phases (Biester & Nehrke, 1997; Biester et al., 1999; Bombach et al., 1994).

4 Conclusions

Application of the sedimentary Hg proxy for volcanic activity is often complicated by the poorly constrained influence of the host-phase for Hg and Hg speciation. Identification of host-phase abundance effects (normalization) is commonly performed by choosing the strongest positive linear relation to common host-phase proxy data (e.g., TOC and TS, the proxies for organic-matter and sulfides). Critically, this approach often relies solely on (linear) correlations to infer which is the most likely host-phase and does not account for any complexity in Hg speciation within or between samples.

We here explore the use of thermal desorption characteristics for geological sediment (rock) samples. Thermal desorption profiles (TDPs) for many Hg species are well-established and a proven tool

to distinguish between OM-bound Hg and different Hg sulfides, as well as Hg-oxides and Hg-selenide (e.g., Bombach et al., 1994; Biester and Nehrke, 1997; Rumayor et al., 2013; Saniewska and Bełdowska, 2017). Using only the rapid (< 3 minute) desorption that is obtained as standard for each sample analyzed in continuous-flow direct Hg analyzers, we illustrate the presence of multiple release-phases (Hg species) in (almost) all of the 65 analyzed sedimentary rock samples of Tithonian (late Jurassic) age (*ca.* 146 – 145 Ma). When examining subsections of the long-term dataset we find that the overall correlation between Hg_T and TOC is much weaker in the here studied interval compared to the more organic-rich shales below.

Invariably, the sediment TDPs that were analyzed show multiple phases of Hg release and these phases occur in different proportions in different samples. We quantify the Hg release in each phase and show the first low-temperature release phase, is likely Hg associated with organic-matter and organic-matter associated sulfides (Hg_{OMS}) whereas a secondary, higher temperature Hg phase that anti-correlates with TOC is of a more enigmatic origin (Hg_{OTH}). Separating Hg_{OMS} and Hg_{OTH} confirms the weak Hg_T (R^2 ~0.2) correlation to TOC corresponds to variable abundance of Hg_{OTH} (Fig. 10B). Specifically, the greater proportion of Hg_{OTH} in carbonate-mudstones may suggest a link to diagenetic effects of Hg and Hg speciation and could suggest the Hg_{OTH} currently hosted in the secondary phases may have been deposited with an OM fraction that has since been oxidized. Such diagenetic effects, that were also observed to focus Hg in pyrite can produce significant stratigraphic enrichments of Hg and warrant caution when interpreting the (normalized) Hg record.

Most importantly, the approach used here demonstrates it is feasible to test for multiple Hg release phases (Hg species) and provides a fast, data-rich, quantitative perspective on Hg behavior in individual sediment samples. Our method allows offline quantification of the individual peaks, which means they can be used flexibly, for example to test whether Hg release phases may or may not align with certain host-phases. As this approach resolves changes in Hg speciation on a sample level, the 'host-phase' identification and quantification does not overly depend on the existence of positive correlation for entire successions and avoids the assumption that all Hg is always hosted in a single phase. Although crude in terms of Hg species identification, the approach can be applied with pyrolysis-based continuous-flow Hg analyzers to any sedimentary Hg record, virtually without additional effort and can be extended to pyrolysis-based analyses with instruments that apply gold-trapping prior to quantification.

Acknowledgments

Funding for this research was provided from an ERC Consolidator Grant (ERC-2018-COG-818717-V-ECHO) to TAM.

Open Research

690 All data and code generated or used to conduct this study are included as supplementary files with the
691 submitted manuscript for review and have been uploaded to a permanent online repository (Figshare, doi:
692 10.6084/m9.figshare.25071032 and 10.6084/m9.figshare.25070576) where they will be made available to
693 the public upon publication.
694

695 ## References

696 Amos, H. M., Jacob, D. J., Kocman, D., Horowitz, H. M., Zhang, Y., Dutkiewicz, S., … Sunderland, E. M. (2014).
697 Global Biogeochemical Implications of Mercury Discharges from Rivers and Sediment Burial. *Environmental*
698 *Science & Technology*, *48*(16), 9514–9522. https://doi.org/10.1021/es502134t
699 Bagnato, E., Tamburello, G., Avard, G., Martinez-Cruz, M., Enrico, M., Fu, X., … Sonke, J. E. (2015). Mercury
700 fluxes from volcanic and geothermal sources: An update. *Geological Society Special Publication*, *410*(1),
701 263–285. https://doi.org/10.1144/SP410.2
702 Bełdowska, M., Saniewska, D., Gębka, K., Kwasigroch, U., Korejwo, E., & Kobos, J. (2018). Simple screening
703 technique for determination of adsorbed and absorbed mercury in particulate matter in atmospheric and
704 aquatic environment. *Talanta*, *182*(October 2017), 340–347. https://doi.org/10.1016/j.talanta.2018.01.082
705 Berner, R. A. (1982). Burial of organic carbon and pyrite sulfur in the modern ocean. *American Journal of Science*.
706 Berner, R. A. (1984). Sedimentary pyrite formation: An update. *Geochimica et Cosmochimica Acta*, *48*(4), 605–615.
707 https://doi.org/10.1016/0016-7037(84)90089-9
708 Biester, H., Gosar, M., & Covelli, S. (2000). Mercury Speciation in Sediments Affected by Dumped Mining
709 Residues in the Drainage Area of the Idrija Mercury Mine, Slovenia. *Environmental Science & Technology*,
710 *34*(16), 3330–3336. https://doi.org/10.1021/es991334v
711 Biester, H., Gosar, M., & Müller, G. (1999). Mercury speciation in tailings of the Idrija mercury mine. *Journal of*
712 *Geochemical Exploration*, *65*(3), 195–204. https://doi.org/10.1016/S0375-6742(99)00027-8
713 Biester, H., & Nehrke, G. (1997). Quantification of mercury in soils and sediments - acid digestion versus pyrolysis.
714 *Fresenius' Journal of Analytical Chemistry*, *358*(3), 446–452. https://doi.org/10.1007/s002160050444
715 Biester, H., & Scholz, C. (1997). Determination of Mercury Binding Forms in Contaminated Soils: Mercury
716 Pyrolysis versus Sequential Extractions. *Environmental Science & Technology*, *31*(1), 233–239.
717 https://doi.org/10.1021/es960369h
718 Biswas, A., Blum, J. D., Klaue, B., & Keeler, G. J. (2007). Release of mercury from rocky mountain forest fires.
719 *Global Biogeochemical Cycles*, *21*(1), 1–13. https://doi.org/10.1029/2006GB002696
720 Bloom, N. S., Preus, E., Katon, J., & Hiltner, M. (2003). Selective extractions to assess the biogeochemically
721 relevant fractionation of inorganic mercury in sediments and soils. *Analytica Chimica Acta*, *479*(2), 233–248.
722 https://doi.org/10.1016/S0003-2670(02)01550-7
723 Bombach, G., Bombach, K., & Klemm, W. (1994). Speciation of mercury in soils and sediments by thermal
724 evaporation and cold vapor atomic absorption. *Fresenius' Journal of Analytical Chemistry*, *350*(1–2), 18–20.
725 https://doi.org/10.1007/BF00326246
726 Chakraborty, P., Raghunadh Babu, P. V., Vudamala, K., Ramteke, D., & Chennuri, K. (2014). Mercury speciation in

coastal sediments from the central east coast of India by modified BCR method. *Marine Pollution Bulletin*, *81*(1), 282–288. https://doi.org/10.1016/j.marpolbul.2013.12.054

Chen, D., Ren, D., Deng, C., Tian, Z., & Yin, R. (2022). Mercury loss and isotope fractionation during high-pressure and high-temperature processing of sediments: Implication for the behaviors of mercury during metamorphism. *Geochimica et Cosmochimica Acta*, *334*, 231–240. https://doi.org/10.1016/j.gca.2022.08.010

Enrico, M., Mere, A., Zhou, H., Loriau, M., Tessier, E., & Bouyssiere, B. (2020). Methods for Total and Speciation Analysis of Mercury in the Petroleum Industry. *Energy & Fuels*, *34*(11), 13307–13320. https://doi.org/10.1021/acs.energyfuels.0c02730

Ernst, R. E., Bond, D. P. G., Zhang, S., Buchan, K. L., Grasby, S. E., Youbi, N., … Doucet, L. S. (2021). Large Igneous Province Record Through Time and Implications for Secular Environmental Changes and Geological Time-Scale Boundaries. In R. E. Ernst, A. J. Dickson, & A. Bekker (Eds.), *Large Igneous Provinces: A Driver of Global Environmental and Biotic Changes* (pp. 1–26). https://doi.org/10.1002/9781119507444.ch1

Fendley, I. M., Frieling, J., Mather, T. A., Ruhl, M., Hesselbo, S. P., & Jenkyns, H. C. (n.d.). Early Jurassic large igneous province carbon emissions constrained by sedimentary mercury. *Nature Geoscience*. https://doi.org/10.1038/s41561-024-01378-5

Fitzgerald, W. F., Lamborg, C. H., & Hammerschmidt, C. R. (2007). Marine biogeochemical cycling of mercury. *Chemical Reviews*, *107*(2), 641–662. https://doi.org/10.1021/cr050353m

Frieling, J., Mather, T. A., Fendley, I. M., Jenkyns, H. C., Zhao, Z., Dahl, T. W., … Dickson, A. J. (2024). No evidence for a volcanic trigger for late Cambrian carbon-cycle perturbations. *Geology*, *52*(1), 12–16. https://doi.org/10.1130/G51570.1

Frieling, J., Mather, T. A., März, C., Jenkyns, H. C., Hennekam, R., Reichart, G.-J., … van Helmond, N. A. G. M. (2023). Effects of redox variability and early diagenesis on marine sedimentary Hg records. *Geochimica et Cosmochimica Acta*, *351*(October), 78–95. https://doi.org/10.1016/j.gca.2023.04.015

Gagnon, C., Pelletier, É., & Mucci, A. (1997). Behaviour of anthropogenic mercury in coastal marine sediments. *Marine Chemistry*, *59*(1–2), 159–176. https://doi.org/10.1016/S0304-4203(97)00071-6

Gallois, R. (2000). The stratigraphy of the Kimmeridge Clay Formation (Upper Jurassic) in the RGGE Project boreholes at Swanworth Quarry and Metherhills, south Dorset. *Proceedings of the Geologists' Association*, *111*(3), 265–280. https://doi.org/10.1016/S0016-7878(00)80019-X

Gamboa Ruiz, W. L., & Tomiyasu, T. (2015). Distribution of mercury in sediments from Kagoshima Bay, Japan, and its relationship with physical and chemical factors. *Environmental Earth Sciences*, *74*(2), 1175–1188. https://doi.org/10.1007/s12665-015-4104-5

Gehrke, G. E., Blum, J. D., & Meyers, P. A. (2009). The geochemical behavior and isotopic composition of Hg in a mid-Pleistocene western Mediterranean sapropel. *Geochimica et Cosmochimica Acta*, *73*(6), 1651–1665. https://doi.org/10.1016/j.gca.2008.12.012

Geyman, B. M., Thackray, C. P., Jacob, D. J., & Sunderland, E. M. (2023). Impacts of Volcanic Emissions on the Global Biogeochemical Mercury Cycle: Insights From Satellite Observations and Chemical Transport Modeling. *Geophysical Research Letters*, *50*(21), 1–10. https://doi.org/10.1029/2023GL104667

764 Gleyzes, C., Tellier, S., & Astruc, M. (2002). Fractionation studies of trace elements in contaminated soils and
765 sediments: a review of sequential extraction procedures. *TrAC Trends in Analytical Chemistry*, *21*(6–7), 451–
766 467. https://doi.org/10.1016/S0165-9936(02)00603-9
767 Gong, Q., Wang, X., Zhao, L., Grasby, S. E., Chen, Z. Q., Zhang, L., … Li, Z. (2017). Mercury spikes suggest
768 volcanic driver of the Ordovician-Silurian mass extinction. *Scientific Reports*, *7*(1), 1–7.
769 https://doi.org/10.1038/s41598-017-05524-5
770 Grasby, S. E., Them, T. R., Chen, Z., Yin, R., & Ardakani, O. H. (2019). Mercury as a proxy for volcanic emissions
771 in the geologic record. *Earth-Science Reviews*, *196*(June), 102880.
772 https://doi.org/10.1016/j.earscirev.2019.102880
773 Grasby, S. E., Sanei, H., Beauchamp, B., & Chen, Z. (2013). Mercury deposition through the Permo-Triassic Biotic
774 Crisis. *Chemical Geology*, *351*, 209–216. https://doi.org/10.1016/j.chemgeo.2013.05.022
775 Haynes, W.M. (2014). *CRC Handbook of Chemistry and Physics*. (William M. Haynes, Ed.) (85th ed.). CRC Press.
776 https://doi.org/10.1201/b17118
777 Hesselbo, S. P., Ogg, J. G., Ruhl, M., Hinnov, L. A., & Huang, C. J. (2020). The Jurassic Period. In *Geologic Time*
778 *Scale 2020* (pp. 955–1021). Elsevier. https://doi.org/10.1016/B978-0-12-824360-2.00026-7
779 Huang, C., Hesselbo, S. P., & Hinnov, L. (2010). Astrochronology of the late Jurassic Kimmeridge Clay (Dorset,
780 England) and implications for Earth system processes. *Earth and Planetary Science Letters*, *289*(1–2), 242–
781 255. https://doi.org/10.1016/j.epsl.2009.11.013
782 Irwin, H. (1980). Early diagenetic carbonate precipitation and pore fluid migration in the Kimmeridge Clay of
783 Dorset, England. *Sedimentology*, *27*(5), 577–591. https://doi.org/10.1111/j.1365-3091.1980.tb01648.x
784 Irwin, H., Curtis, C., & Coleman, M. (1977). Isotopic evidence for source of diagenetic carbonates formed during
785 burial of organic-rich sediments. *Nature*, *269*(5625), 209–213. https://doi.org/10.1038/269209a0
786 Issaro, N., Abi-Ghanem, C., & Bermond, A. (2009). Fractionation studies of mercury in soils and sediments: A
787 review of the chemical reagents used for mercury extraction. *Analytica Chimica Acta*, *631*(1), 1–12.
788 https://doi.org/10.1016/j.aca.2008.10.020
789 Jenkyns, H. C., Coe, A. L., Gallois, R., Hesselbo, S. P., Marshall, J. E. A., Morgans-Bell, H. S., … Williams, C. J.
790 (2001). *Data from the NERC Rapid Global Geological Events (RGGE) programme for Swanworth Quarry 1*
791 *and Metherhills 1 boreholes.* https://doi.org/10.5285/a8e86b5e-f341-419e-be98-0463efe3201f
792 Jiskra, M., Desgranges, M., & Petrova, M. V. (2021). Mercury stable isotopes constrain atmospheric sources to the
793 Ocean. *Nature*, *597*(September). https://doi.org/10.1038/s41586-021-03859-8
794 Jones, M. T., Percival, L. M. E., Stokke, E. W., Frieling, J., Mather, T. A., Riber, L., … Svensen, H. H. (2019).
795 Mercury anomalies across the Palaeocene–Eocene Thermal Maximum. *Climate of the Past*, *15*(1), 217–236.
796 https://doi.org/10.5194/cp-15-217-2019
797 Van Kaam-Peters, H. M. E., Schouten, S., Köster, J., & Damstè, J. S. S. (1998). Controls on the molecular and
798 carbon isotopic composition of organic matter deposited in a Kimmeridgian euxinic shelf sea: Evidence for
799 preservation of carbohydrates through sulfurisation. *Geochimica et Cosmochimica Acta*, *62*(19–20), 3259–
800 3283. https://doi.org/10.1016/S0016-7037(98)00231-2

Kim, C. S., Bloom, N. S., Rytuba, J. J., & Brown, G. E. (2003). Mercury Speciation by X-ray Absorption Fine Structure Spectroscopy and Sequential Chemical Extractions: A Comparison of Speciation Methods. *Environmental Science and Technology*, *37*(22), 5102–5108. https://doi.org/10.1021/es0341485

Kodrans-Nsiah, M., März, C., Harding, I. C., Kasten, S., & Zonneveld, K. A. F. (2009). Are the Kimmeridge Clay deposits affected by "burn-down" events? Palynological and geochemical studies on a 1 metre long section from the Upper Kimmeridge Clay Formation (Dorset, UK). *Sedimentary Geology*, *222*(3–4), 301–313. https://doi.org/10.1016/j.sedgeo.2009.09.015

Kovács, E. B., Ruhl, M., Silva, R. L., McElwain, J. C., Reolid, M., Korte, C., … Hesselbo, S. P. (2024). Mercury sequestration pathways under varying depositional conditions during Early Jurassic (Pliensbachian and Toarcian) Karoo-Ferrar volcanism. *Palaeogeography, Palaeoclimatology, Palaeoecology*, *637*(October 2023), 111977. https://doi.org/10.1016/j.palaeo.2023.111977

Leipe, T., Moros, M., Kotilainen, A., Vallius, H., Kabel, K., Endler, M., & Kowalski, N. (2013). Mercury in Baltic Sea sediments-Natural background and anthropogenic impact. *Chemie Der Erde*, *73*(3), 249–259. https://doi.org/10.1016/j.chemer.2013.06.005

Lim, D., Kim, H., Kim, J., Jeong, D., & Kim, D. (2020). Mercury proxy for hydrothermal and submarine volcanic activities in the sediment cores of Central Indian Ridge. *Marine Pollution Bulletin*, *159*(July), 1–8. https://doi.org/10.1016/j.marpolbul.2020.111513

Liu, Z., Tian, H., Yin, R., Chen, D., & Gai, H. (2022). Mercury loss and isotope fractionation during thermal maturation of organic-rich mudrocks. *Chemical Geology*, *612*, 121144. https://doi.org/10.1016/j.chemgeo.2022.121144

Lyman, S. N., Cheng, I., Gratz, L. E., Weiss-Penzias, P., & Zhang, L. (2020). An updated review of atmospheric mercury. *Science of the Total Environment*, *707*, 135575. https://doi.org/10.1016/j.scitotenv.2019.135575

Machado, W., Sanders, C. J., Santos, I. R., Sanders, L. M., Silva-Filho, E. V., & Luiz-Silva, W. (2016). Mercury dilution by autochthonous organic matter in a fertilized mangrove wetland. *Environmental Pollution*, *213*, 30–35. https://doi.org/10.1016/j.envpol.2016.02.002

Manceau, A., Merkulova, M., Murdzek, M., Batanova, V., Baran, R., Glatzel, P., … Lefticariu, L. (2018). Chemical Forms of Mercury in Pyrite: Implications for Predicting Mercury Releases in Acid Mine Drainage Settings. *Environmental Science and Technology*, *52*(18), 10286–10296. https://doi.org/10.1021/acs.est.8b02027

Matthews, A., Morgans-Bell, H. S., Emmanuel, S., Jenkyns, H. C., Erel, Y., & Halicz, L. (2004). Controls on iron-isotope fractionation in organic-rich sediments (Kimmeridge Clay, Upper Jurassic, Southern England). *Geochimica et Cosmochimica Acta*, *68*(14), 3107–3123. https://doi.org/10.1016/j.gca.2004.01.019

Mercone, D., Thomson, J., Croudace, I. ., & Troelstra, S. . (1999). A coupled natural immobilisation mechanism for mercury and selenium in deep-sea sediments. *Geochimica et Cosmochimica Acta*, *63*(10), 1481–1488. https://doi.org/10.1016/S0016-7037(99)00063-0

Morgans-Bell, H. S., Coe, A. L., Hesselbo, S. P., Jenkyns, H. C., Weedon, G. P., Marshall, J. E. A., … Williams, C. J. (2001). Integrated stratigraphy of the Kimmeridge Clay Formation (Upper Jurassic) based on exposures and boreholes in south Dorset, UK. *Geological Magazine*, *138*(5), 511–539.

https://doi.org/10.1017/S0016756801005738

Outridge, P. M., Sanei, H., Stern, G. A., Hamilton, P. B., & Goodarzi, F. (2007). Evidence for control of mercury accumulation rates in Canadian High Arctic Lake sediments by variations of aquatic primary productivity. *Environmental Science and Technology*, *41*(15), 5259–5265. https://doi.org/10.1021/es070408x

Percival, L. M. E., Witt, M. L. I., Mather, T. A., Hermoso, M., Jenkyns, H. C., Hesselbo, S. P., … Ruhl, M. (2015). Globally enhanced mercury deposition during the end-Pliensbachian extinction and Toarcian OAE: A link to the Karoo–Ferrar Large Igneous Province. *Earth and Planetary Science Letters*, *428*, 267–280. https://doi.org/10.1016/j.epsl.2015.06.064

Percival, L. M. E., Bergquist, B. A., Mather, T. A., & Sanei, H. (2021). Sedimentary Mercury Enrichments as a Tracer of Large Igneous Province Volcanism. In R. E. Ernst, A. J. Dickson, & A. Bekker (Eds.), *Large Igneous Provinces: A Driver of Global Environmental and Biotic Changes* (pp. 247–262). Geophysical Monograph Series, American Geophysical Union. https://doi.org/10.1002/9781119507444.ch11

Percival, L. M. E., Ruhl, M., Hesselbo, S. P., Jenkyns, H. C., Mather, T. A., & Whiteside, J. H. (2017). Mercury evidence for pulsed volcanism during the end-Triassic mass extinction. *Proceedings of the National Academy of Sciences of the United States of America*, *114*(30), 7929–7934. https://doi.org/10.1073/pnas.1705378114

Percival, L. M. E., Jenkyns, H. C., Mather, T. A., Dickson, A. J., Batenburg, S. J., Ruhl, M., … Woelders, L. (2018). Does large igneous province volcanism always perturb the mercury cycle? Comparing the records of Oceanic Anoxic Event 2 and the end-Cretaceous to other Mesozoic events. *American Journal of Science*, *318*(8), 799–860. https://doi.org/10.2475/08.2018.01

Petranich, E., Predonzani, S., Acquavita, A., Mashyanov, N., & Covelli, S. (2022). Applied Geochemistry Rapid thermoscanning technique for direct analysis of mercury species in contaminated sediments : From pure compounds to real sample application. *Applied Geochemistry*, *143*(July), 105393. https://doi.org/10.1016/j.apgeochem.2022.105393

Pham, A. L. T., Morris, A., Zhang, T., Ticknor, J., Levard, C., & Hsu-Kim, H. (2014). Precipitation of nanoscale mercuric sulfides in the presence of natural organic matter: Structural properties, aggregation, and biotransformation. *Geochimica et Cosmochimica Acta*, *133*, 204–215. https://doi.org/10.1016/j.gca.2014.02.027

Pyle, D. M., & Mather, T. A. (2003). The importance of volcanic emissions for the global atmospheric mercury cycle. *Atmospheric Environment*, *37*(36), 5115–5124. https://doi.org/10.1016/j.atmosenv.2003.07.011

Raiswell, R., Newton, R., & Wignall, P. B. (2001). An Indicator of Water-Column Anoxia: Resolution of Biofacies Variations in the Kimmeridge Clay (Upper Jurassic, U.K.). *Journal of Sedimentary Research*, *71*(2), 286–294. https://doi.org/10.1306/070300710286

Rakociński, M., Marynowski, L., Pisarzowska, A., Bełdowski, J., Siedlewicz, G., Zatoń, M., … Schönlaub, H. P. (2020). Volcanic related methylmercury poisoning as the possible driver of the end-Devonian Mass Extinction. *Scientific Reports*, *10*(1), 1–8. https://doi.org/10.1038/s41598-020-64104-2

Raven, M. R., Crockford, P. W., Hodgskiss, M. S. W., Lyons, T. W., Tino, C. J., & Webb, S. M. (2023). Organic matter sulfurization and organic carbon burial in the Mesoproterozoic. *Geochimica et Cosmochimica Acta*,

347, 102–115. https://doi.org/10.1016/j.gca.2023.02.020

Ravichandran, M. (2004). Interactions between mercury and dissolved organic matter - A review. *Chemosphere*, *55*(3), 319–331. https://doi.org/10.1016/j.chemosphere.2003.11.011

Reis, A. T., Coelho, J. P., Rucandio, I., Davidson, C. M., Duarte, A. C., & Pereira, E. (2015). Thermo-desorption: A valid tool for mercury speciation in soils and sediments? *Geoderma*, *237*, 98–104. https://doi.org/10.1016/j.geoderma.2014.08.019

Rumayor, M., Gallego, J. R., Rodríguez-Valdés, E., & Díaz-Somoano, M. (2017). An assessment of the environmental fate of mercury species in highly polluted brownfields by means of thermal desorption. *Journal of Hazardous Materials*, *325*, 1–7. https://doi.org/10.1016/j.jhazmat.2016.11.068

Rumayor, M., Diaz-Somoano, M., Lopez-Anton, M. A., & Martinez-Tarazona, M. R. (2013). Mercury compounds characterization by thermal desorption. *Talanta*, *114*, 318–322. https://doi.org/10.1016/j.talanta.2013.05.059

Rumayor, M., Diaz-Somoano, M., Lopez-Anton, M. A., & Martinez-Tarazona, M. R. (2015). Application of thermal desorption for the identification of mercury species in solids derived from coal utilization. *Chemosphere*, *119*, 459–465. https://doi.org/10.1016/j.chemosphere.2014.07.010

Rumayor, M., Lopez-Anton, M. A., Díaz-Somoano, M., & Martínez-Tarazona, M. R. (2015). A new approach to mercury speciation in solids using a thermal desorption technique. *Fuel*, *160*, 525–530. https://doi.org/10.1016/j.fuel.2015.08.028

Rumayor, M., Lopez-Anton, M. A., Díaz-Somoano, M., Maroto-Valer, M. M., Richard, J.-H., Biester, H., & Martínez-Tarazona, M. R. (2016). A comparison of devices using thermal desorption for mercury speciation in solids. *Talanta*, *150*, 272–277. https://doi.org/10.1016/j.talanta.2015.12.058

Sanei, H., Grasby, S. E., & Beauchamp, B. (2012). Latest Permian mercury anomalies. *Geology*, *40*(1), 63–66. https://doi.org/10.1130/G32596.1

Saniewska, D., & Bełdowska, M. (2017). Mercury fractionation in soil and sediment samples using thermo-desorption method. *Talanta*, *168*(January), 152–161. https://doi.org/10.1016/j.talanta.2017.03.026

Schuster, P. F., Schaefer, K. M., Aiken, G. R., Antweiler, R. C., Dewild, J. F., Gryziec, J. D., … Zhang, T. (2018). Permafrost Stores a Globally Significant Amount of Mercury. *Geophysical Research Letters*, *45*(3), 1463–1471. https://doi.org/10.1002/2017GL075571

Scotchman, I. C. (1991). The geochemistry of concretions from the Kimmeridge Clay Formation of southern and eastern England. *Sedimentology*, *38*(1), 79–106. https://doi.org/10.1111/j.1365-3091.1991.tb01856.x

Selin, N. E. (2009). Global Biogeochemical Cycling of Mercury: A Review. *Annual Review of Environment and Resources*, *34*(1), 43–63. https://doi.org/10.1146/annurev.environ.051308.084314

Shen, J., Feng, Q., Algeo, T. J., Liu, J., Zhou, C., Wei, W., … Chen, J. (2020). Sedimentary host phases of mercury (Hg) and implications for use of Hg as a volcanic proxy. *Earth and Planetary Science Letters*, *543*, 116333. https://doi.org/10.1016/j.epsl.2020.116333

Shen, J., Algeo, T. J., Chen, J., Planavsky, N. J., Feng, Q., Yu, J., & Liu, J. (2019). Mercury in marine Ordovician/Silurian boundary sections of South China is sulfide-hosted and non-volcanic in origin. *Earth and Planetary Science Letters*, *511*, 130–140. https://doi.org/10.1016/j.epsl.2019.01.028

912 Svensen, H. H., Jones, M. T., Percival, L. M. E., Grasby, S. E., & Mather, T. A. (2023). Release of mercury during
913 contact metamorphism of shale : Implications for understanding the impacts of large igneous province
914 volcanism. *Earth and Planetary Science Letters*, *619*, 118306. https://doi.org/10.1016/j.epsl.2023.118306
915 Tyson, R. V., Wilson, R. C. L., & Downie, C. (1979). A stratified water column environmental model for the type
916 Kimmeridge Clay [10]. *Nature*. https://doi.org/10.1038/277377a0
917 Wallace, G. T. (1982). The association of copper, mercury and lead with surface-active organic matter in coastal
918 seawater. *Marine Chemistry*, *11*, 379–394.
919 Wang, Y., Tan, J., Wang, W., Zhou, L., Tang, P., Kang, X., … Dick, J. (2023). The influence of Late Ordovician
920 volcanism on the marine environment based on high-resolution mercury data from South China. *GSA Bulletin*,
921 *135*(3–4), 787–798. https://doi.org/10.1130/b36257.1
922 Wang, Z., Tan, J., Boyle, R., Wang, W., Kang, X., Dick, J., & Lyu, Q. (2020). Mercury anomalies within the lower
923 Cambrian (stage 2–3) in South China: Links between volcanic events and paleoecology. *Palaeogeography,*
924 *Palaeoclimatology, Palaeoecology*, *558*(April). https://doi.org/10.1016/j.palaeo.2020.109956
925 Weedon, G. P., Jenkyns, H. C., Coe, A. L., & Hesselbo, S. P. (1999). Astronomical calibration of the Jurassic time-
926 scale from cyclostratigraphy in British mudrock formations. *Philosophical Transactions of the Royal Society*
927 *A: Mathematical, Physical and Engineering Sciences*, *357*(1757), 1787–1813.
928 https://doi.org/10.1098/rsta.1999.0401
929 Werne, J. P., Lyons, T. W., Hollander, D. J., Formolo, M. J., & Sinninghe Damsté, J. S. (2003). Reduced sulfur in
930 euxinic sediments of the Cariaco Basin: Sulfur isotope constraints on organic sulfur formation. *Chemical*
931 *Geology*, *195*(1–4), 159–179. https://doi.org/10.1016/S0009-2541(02)00393-5
932 Williams, C. J., Hesselbo, S. P., Jenkyns, H. C., & Morgans-Bell, H. S. (2001). Quartz silt in mudrocks as a key to
933 sequence stratigraphy (Kimmeridge Clay Formation, Late Jurassic, Wessex Basin, UK). *Terra Nova*, *13*(6),
934 449–455. https://doi.org/10.1046/j.1365-3121.2001.00378.x
935 Wilman, B., Saniewska, D., Pyta, H., Wysiecki, D., & Bełdowska, M. (2023). Mercury fractionation - Problems in
936 method application. *Marine Pollution Bulletin*, *187*(January). https://doi.org/10.1016/j.marpolbul.2022.114560
937 Yudovich, Y. E., & Ketris, M. P. (2005). Mercury in coal: A review. Part 1. Geochemistry. *International Journal of*
938 *Coal Geology*, *62*(3), 107–134. https://doi.org/10.1016/j.coal.2004.11.002
939 Zaputlyaeva, A., Mazzini, A., Blumenberg, M., Scheeder, G., Kürschner, W. M., Kus, J., … Frieling, J. (2020).
940 Recent magmatism drives hydrocarbon generation in north-east Java, Indonesia. *Scientific Reports*, *10*(1),
941 1786. https://doi.org/10.1038/s41598-020-58567-6
942 Zhao, H., Grasby, S. E., Wang, X., Zhang, L., Liu, Y., Chen, Z., … Huang, Y. (2022). Mercury enrichments during
943 the Carnian Pluvial Event (Late Triassic) in South China. *GSA Bulletin*, *134*(9–10), 2709–2720.
944 https://doi.org/10.1130/B36205.1
945